THE DESIGN OF A COMPACT ACTUATOR SYSTEM FOR A ROBOTIC WRIST/HAND

by

Catherine J. Anderson

B.S. Mechanical Engineering
Massachusetts Institute of Technology (1990)

Submitted to the Department of
Mechanical Engineering in Partial Fulfillment of
the Requirements for the Degree of

MASTER OF SCIENCE

at the

Massachusetts Institute of Technology

February 1992

Signature of Author 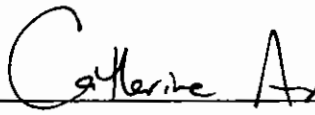
Department of Mechanical Engineering
January 15th, 1992

Certified by 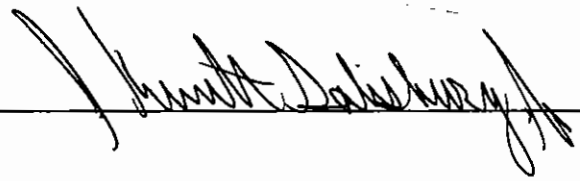
J. Kenneth Salisbury, Jr.
Principal Research Scientist
Thesis Supervisor

Accepted by _____
Ain A. Sonin
Chairman, Departmental Graduate Committee

THE DESIGN OF A COMPACT ACTUATOR SYSTEM FOR A ROBOTIC WRIST/HAND

by

Catherine J. Anderson

Submitted to the Department of Mechanical Engineering
on January 17th, 1992 in partial fulfillment of
the requirements for the Degree of Master of Science

ABSTRACT

This thesis presents the design and implementation of a compact, light-weight actuator package for a cable-driven robotic hand and wrist to be attached to the MIT WAM (Whole Arm Manipulator).

The key features of this actuator package and wrist/hand are high-bandwidth response to disturbance forces, high speed, and high strength.

A process for choosing motors for servo applications is developed and presented. A survey of polymer cable materials including Spectra™ and Vectran™ was performed. A series of fatigue and creep experiments were verified for small cable diameters.

Data from preliminary testing is presented, showing that the hand/wrist and actuators are robust and resistant to abuse while still meeting the design constraints.

This work was done in conjunction with Thomas H. Moyer, M.S.M.E. 1992.

Thesis Supervisor: Dr. J. Kenneth Salisbury, Jr.

Title: Principal Research Scientist

Acknowledgements

Thanks guys, you know who you are.

This research was conducted in the Robotics group at the Artificial Intelligence Laboratory of the Massachusetts Institute of Technology. Support for this research is provided by NASA contract number NAG-9-319 and by the University Research Initiative Program under Office of Naval Research Contract N00014-86-K-0685.

Table of Contents

1.0 Introduction.....9
1.1 A guide to the thesis.....12
1.2 The Hand.....13
2.0 Hand vs. Arm: Performance Tradeoffs.....17
2.1 Bandwidth.....18
2.2 Backdriveability.....22
2.3 Speed and Inertia Tradeoffs.....22
3.0 System Specifications.....39
3.1 Size.....39
3.2 Number of Actuators.....40
3.3 Gripper Speed and Acceleration.....41
3.4 Strength and Power.....43
3.5 Arm Speed and Hand Bandwidth.....44
3.6 Mass of the Forearm.....45
3.7 Backdriveability.....46
3.8 Sensor Requirements.....46
3.9 Maintenance.....47
3.10 Summary.....48
4.0 Design Alternatives.....49
4.1 Actuation Methods.....49
4.2 Transmissions.....50
4.3 Configurations.....50
4.4 Bias Torques.....54
4.5 Making the Optimum Motor Choice.....58
4.6 Cable Materials.....66
5.0 The Design of the Actuator Package.....75
5.1 Motor modifications.....75
5.2 Actuator Package Layout and Construction.....76
6.0 Implementation of the Tendon Tension Control Loop.....83
7.0 Results.....87
8.0 Future work.....91
8.1 Pulley Keepers.....91
8.2 Slack Prevention Springs.....92
8.3 Cable passage in 3D.....92
8.4 Cable Experiments.....92
8.5 Finishing the Wrist and Attaching it to the WAM.....92
Appendix A Motor data comparisons.....95
Appendix B More Mechanical Drawings.....99
Bibliography.....103

List of Figures

Figure 1.0.1 MIT Whole Arm Manipulator 10
Figure 1.0.2 WAM grasping an object 11
Figure 1.2.1 Picture of Current Hand 13
Figure 1.2.2 A Prototype of the WAM wrist/hand 14
Figure 1.2.3 2n cabling for a 2 DOF 2 link finger 15
Figure 1.2.4 n+1 cabling for a 2 DOF 2 link finger 15

Figure 2.1.1 Model of the Robot with Motor and Link Inertia, ... 19
Figure 2.3.1 WAM Plane of Motion to be Modeled. 23
Figure 2.3.2 Free Body Diagram of the Planar revolute robot 26
Figure 2.3.3 Model of the first Link 29
Figure 2.3.4 Model of the Second Link 30
Figure 2.3.5 The Effect of Gravity on Acceleration of the WAM. 33
Figure 2.3.6 Acceleration Capability (in ft/sec2) of the WAM 34

Figure 3.1.1 The WAM Gripping a Ball with the Inner Reaction Surface 40
Figure 3.3.1 Equivalent Mass for a Rotational Inertia 41
Figure 3.3.2 Several Velocity Profiles for Moving 6 inches in 150 ms 42
Figure 3.4.1 Tendon Tension for the Wrist/Hand Cables vs. Force Angle 43

Figure 4.3.1 Perpendicular and Axial Motor Configuration 51
Figure 4.3.2 Different Six Actuator Bundles for Varying Sizes of Actuators 51
Figure 4.3.3 Ring Motor 52
Figure 4.3.4 The Stack Configuration for Ring Motors 53
Figure 4.4.1 Bias torque using a c-force spring 54
Figure 4.4.2 Spring force in lbs. vs. stock thickness and spool diameter in inches 56
Figure 4.4.3 Weight of Springs (in oz) to meet 40 lb. Force Requirement 57
Figure 4.5.1 Acceleration Profiles with Velocity Dependant Accelerations. 63
Figure 4.6.1 Elongation of 150 lb.Test Spectra 900 Cable vs.Time 70
Figure 4.6.2 Stress Relaxation in Spectra 900, Kevlar 29, and Vectran HS 71
Figure 4.6.3 Cable Fatigue Testing Apparatus 72
Figure 4.6.4 Self-Abrasion Life of 150 lb. Test Spectra 900 Cable. 72
Figure 4.6.5 Bend-Over-Sheave Test on Spectra 900, Kevlar 29 73

Figure 5.1.1 Crossections of the New and Old Endcaps 76
Figure 5.1.2 Closest Packing for Motors with Encoders 77
Figure 5.1.3 Pulley Mounts with Strain Gauge Attachments. 78
Figure 5.1.4 Wrap Angle (Q),Center Distance (d), ... 79
Figure 5.1.5 Top Plate of Actuator Package with Cable Distances Maximized 79
Figure 5.1.6 Exploded View of the Actuator Package. 80
Figure 5.1.7 The Assembled Actuator Package During Preliminary Testing 82

Figure 6.0.1 Pulley Mount with Strain Gauges 83
Figure 6.0.2 Tendon Tension Testing Setup..... 84
Figure 6.0.3 Open Loop Force Trajectory. 85
Figure 6.0.4 Force Feedback for Closing the Torque Loop..... 85
Figure 6.0.5 Force Trajectory with a Force Feedback Gain of 60..... 85
Figure 6.0.5 Error Comparison Between Open Loop Trajectory and Force Feedback With a Gain of 60.. 86

Figure 7.0.1 The Forearm Mockup with the the Actuator Package..... 88
Figure 7.0.2 The Hand Grasping a Stapler. 89

Figure 8.1.1 Pulley Mount with Keeper..... 91
Figure 8.3.1WAM with Proposed Forearm..... 93

Figure A1. Upper Faceplate of the Actuator Package Gearbox..... 99
Figure A2. Lower Faceplate of the Actuator Package Gearbox..... 100
Figure A3. Pulley Mount..... 101

List of Tables

Table 2.3.1 WAM and Hand/Wrist Parameters used for Model..... 32
Table 4.5.1. Physical Constraints on the Motors..... 59
Table 4.6.1 Density, Tenacity and Modulus Data for Several Cable Materials 69
Table A1. Motor Data Comparisons..... 95

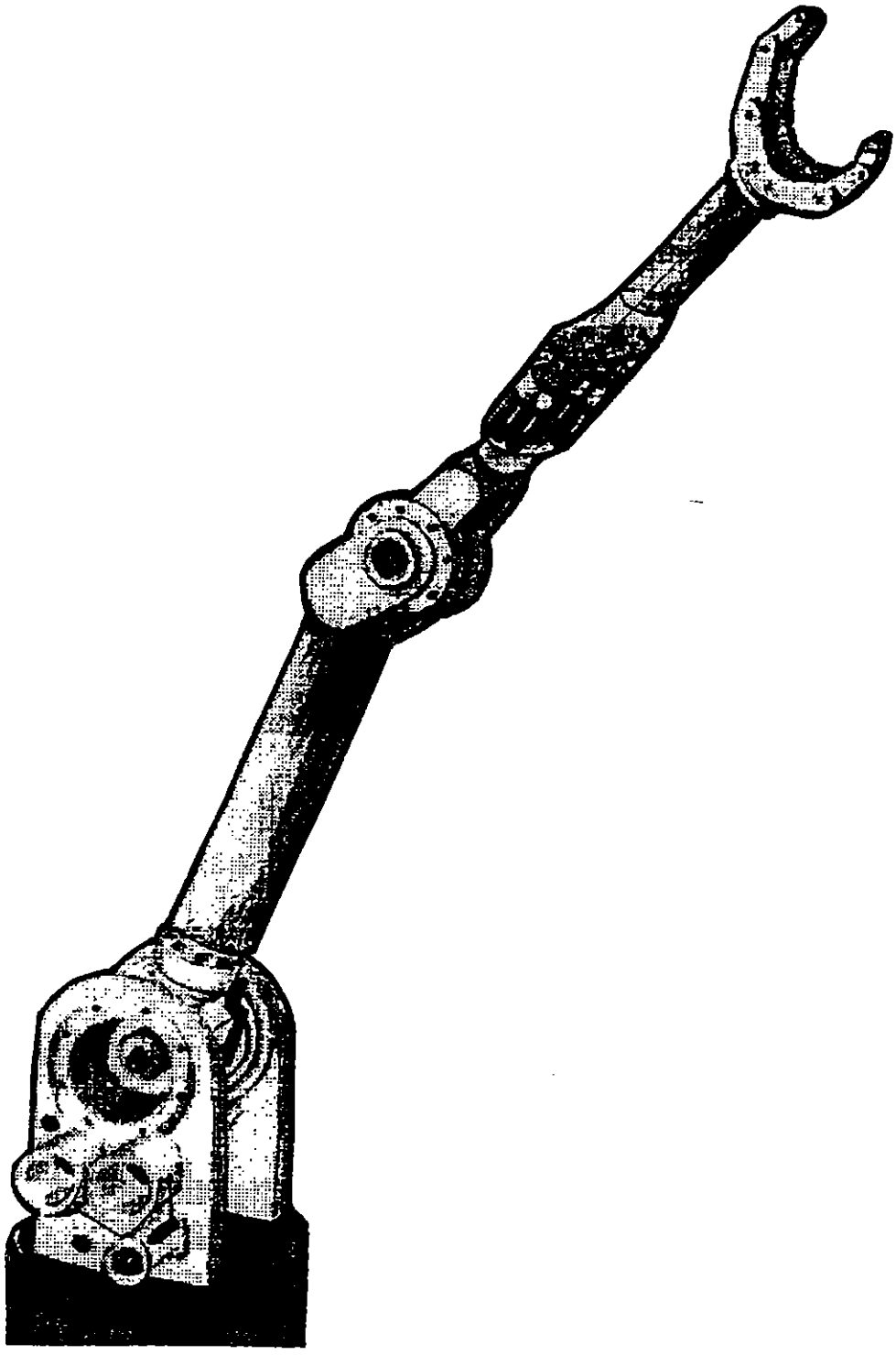

1.0 Introduction.

This thesis deals with the design and construction of an actuator package for an articulated gripper and wrist designed by [Moyer, 92]. The gripper, wrist, and actuator package were designed to be retrofitted to the MIT Whole Arm Manipulator (WAM) (see figure 1.0.1) which was designed and built by the WAM group at the MIT Artificial Intelligence Laboratory [Salisbury, 88], [Townsend, 88], [Eberman, 89], and [DiPietro, 88].

There are several aspects of the robot arm and the articulated gripper which make adding an actuator package to the forearm a non-trivial task. First, Whole-Arm Manipulation differs from other areas of robotics in that all of the surfaces of the robot arm are used in contact with the environment (as opposed to an arm serving only as an end effector positioner) (see Figure 1.0.2). This requires that the actuator package for the hand fit inside the existing (slender) robot surfaces, and not have any external tubes or wires that can get snagged by the environment.

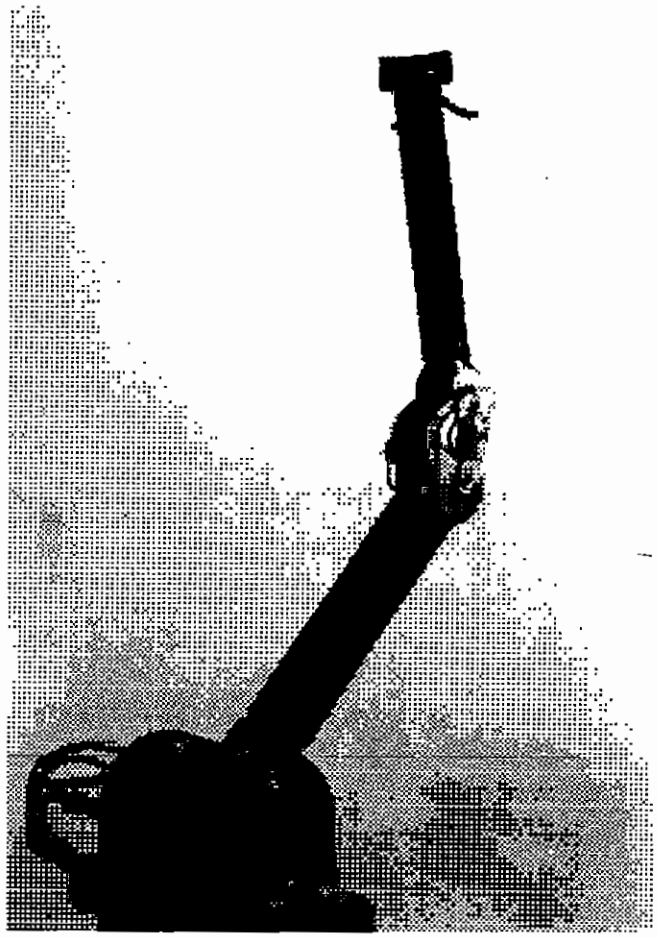

Figure 1.0.1 MIT Whole Arm Manipulator

Also, there are severe restrictions on the mass of the actuators and gripper. A gripper and actuator similar to many of the existing multi degree of freedom (DOF) hand designs such as the Utah/MIT hand [Jacobsen et al, 86], the Salisbury hand (aka Stanford-JPL hand) [Mason and Salisbury, 85], would slow the arm down greatly. We are especially concerned with speed and acceleration because we want to use the fast dynamics of the arm to accomplish tasks such as throwing and catching (possibly tumbling) objects.

With these two major restrictions and the overall design of the hand aimed at quick reliable grasping rather than so called "dexterous" manipulation, the major questions addressed by this thesis are:

1. What performance is required of a wrist/hand system so that it compliments an existing arm

2. How to most effectively implement this design

Figure 1.0.2. WAM grasping an object

1.1 A guide to the thesis

The last section of this chapter contains information about the articulated gripper and wrist that are to be driven by the actuator package, while the remainder of the thesis is divided into the following chapters:

2.0 Hand vs. Arm: Performance Tradeoffs. This chapter describes the characteristics used to define and measure "performance", and the interdependence of the hand and arm's performance. A model for the WAM's dynamics in a subset of the workspace is developed in section 2.3 and used to predict the robot behavior with the additional mass of an actuator package.

3.0 System Specifications. Using some of the data from the performance models, and additional physical and performance requirements, the system specifications for the actuator package are defined.

4.0 Design Alternatives. This section explores some of the alternatives that were considered during the design of the actuator package. The discarded designs that may be useful for slightly different applications are presented here. In addition, a procedure for choosing motors for servo applications is detailed in section 4.5.

5.0 The Actuator Package Design. Is a description of design and construction details of the actuator package.

6.0 The Tension Control Loop. Includes techniques and experimental results from closed loop torque control of one of the permanent magnet DC motors used to actuate the hand. This was done to reduce the motor's torque ripple and increase the accuracy of the force control of the hand.

7.0 Results. Some experimental results from the prototype forearm with the actuator package and the hand.

8.0 Conclusions. Conclusions about the design based upon the results, with suggestions for future work and design improvements.

Note, since the United States is still in transition between the archaic "slug-foot-second" system of measurement and the internationally accepted SI, both American and International standard units are presented.

1.2 The Hand

The WAM is currently fitted with a 1 degree of freedom (DOF) pneumatic gripper (see Figure 1.2.1) that weighs 1 lb.[.45 Kg] This hand allows the WAM to catch some objects, but it is severely limited in this ability because it does not have a wrist to aid in gripper orientation.

Figure 1.2.1 Picture of Current Hand.

The new articulated wrist/hand that is to be fitted to the WAM (hereafter referred to as the WAM hand or the wrist/hand), is a 2 DOF, two finger, passively curling gripper with a 3 DOF wrist, designed by [Moyer, 92]. The passively curling fingers are based upon the "Prehensile Acquisition Linkage Mechanism" (PALM) developed by [Greiner, 90]. It is designed to be very light and robust, and be capable of capturing objects in a stable grasp without detailed prior knowledge of the object's shape. This characteristic

makes the hand a robust grasper rather than a dexterous manipulator such as the Salisbury hand [Mason and Salisbury, 85]. A prototype of the wrist/hand is shown in Figure 1.2.2.

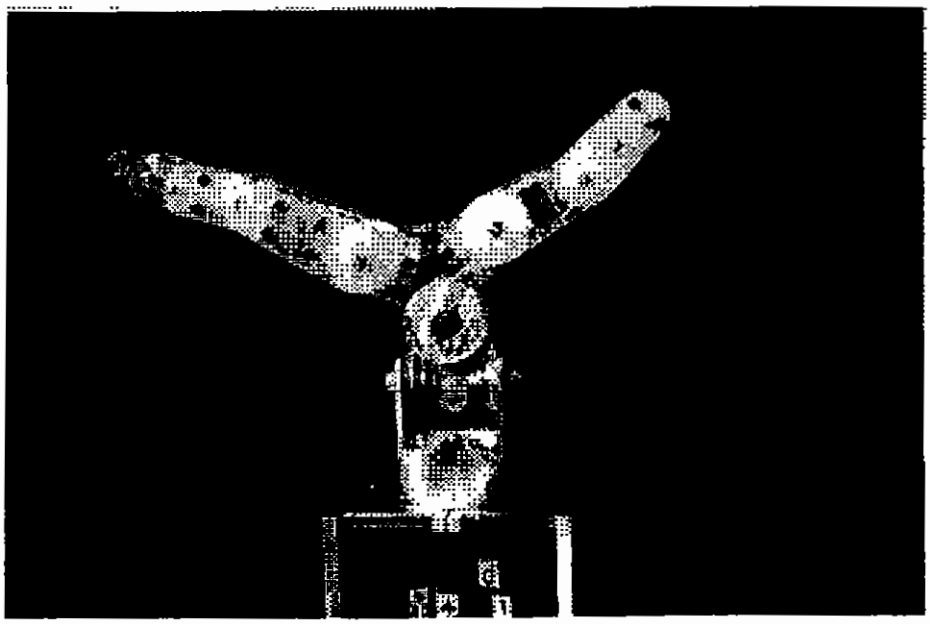

Fig. 1.2.2. A Prototype of the WAM wrist/hand.

The hand is designed to be actuated with cables thereby allowing the actuators to be placed away from the hand. This distance decreases the mass at the end of the "forearm" link, reduces angular inertia and (we hope) will help maintain the WAM's fast dynamics. The cabling method for the hand is an "*n+1*" design developed by Salisbury [Mason and Salisbury, 85] for the Salisbury hand (the *n+1* refers to the number of tendons required to actuate a device with *n* DOF). In an *n+1* cabling system, each DOF is actuated by a combination of tendons (see Figure 1.2.3). In contrast, a 2*n* system has each DOF actuated by an independent set of two cables working in opposition (see Figure 1.2.4). Although the coupled nature of the *n+1* cabling makes the hand less intuitive to design and control, the main advantage of this system is that the pre-tension in the cables may be actively controlled (eliminating the problem of cable stretch and creep). The 2*n* cabling must either have two cables run from one actuator with no active retensioning (as the cable

stretches, the pretension diminishes), or have one actuator for each cable, doubling the number of actuators necessary for the design. See [Moyer, 92] for a complete description of the cabling for the WAM wrist/hand.

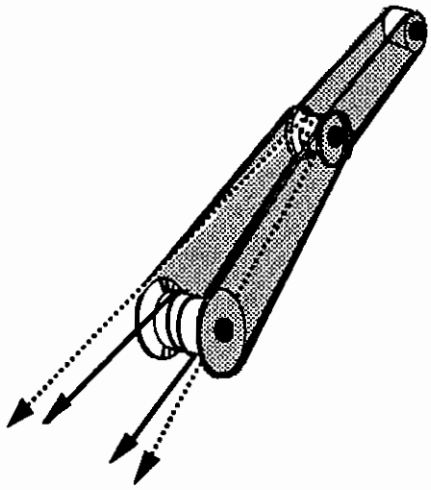

Figure 1.2.3. $2n$ cabling for a 2 DOF 2 link finger

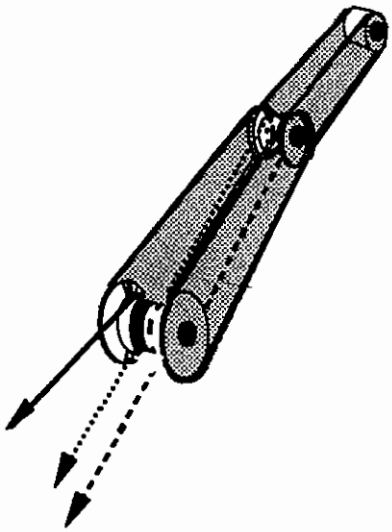

Figure 1.2.4 $n+1$ cabling for a 2 DOF 2 link finger.

2.0 Hand vs. Arm: Performance Tradeoffs

While meeting its own performance criteria, it is important that the weight of the new hand and actuator package not compromise the performance of the WAM. If the actuator package mass is such that the arm can no longer accelerate and move quickly, then the new hand and wrist that were meant to improve catching, will hamper the arm to the extent that it will only be able to catch objects thrown directly at the hand. Before we can estimate how much performance degradation we can tolerate, we need to define the desirable characteristics of the robot and determine how they are affected by adding the mass of an actuator package.

For the WAM and the WAM wrist/hand, the traditional measures of robot quality (accuracy, repeatability, stability) do not tell the whole story. We must also look carefully at bandwidth, backdriveability and acceleration. It is the combination of these which describe the most important attributes of the WAM and the WAM wrist/hand. This chapter describes these characteristics, and the interdependence of the hand and arm performance. In sections 2.1 and 2.2 mechanical bandwidth and backdriveabliliy are examined, and in section 2.3 a model for the dynamics in a subset of the workspace is developed and used to predict how the WAM will behave with the additional mass of an actuator package. This model of the WAM performance, with and without the additional mass of the new hand/wrist, is then used to develop some of the design specifications for the hand actuator package.

2.1 Bandwidth

The bandwidth of a robot is a measure of how quickly the actuator positions and forces are transmitted through the links to the end effector. High bandwidth is desirable for force control, [Whitney, 87] and although high bandwidths are possible with force and position feedback [Hogan, 87], high actuator torques are required to drive the system with the desired response if the mechanical bandwidth is low [Townsend, 88]. Since the mechanical bandwidth is dependant primarily on the stiffness and mass of the system, a robot (or robot hand and wrist) that is intended to be fast must be designed with high bandwidth from the beginning* .

In the case of the WAM, the transmission was designed to be optimally stiff for a forearm with higher inertia than the original lightweight carbon forearm (up to 2 Kg at the endpoint) [Townsend, 88]. This stiff transmission was designed in anticipation of adding some kind of gripper to the WAM. Had the transmission not been "too stiff", the additional weight of the gripper would have reduced the bandwidth of the arm. This additional inertia capacity is for the gripper *and* its payload, however, meaning any mass we add to the gripper detracts from our maximum payload. Unfortunately, the very small, light motors we would choose keep the mass low, tend to be low power, and would be sluggish when moving the hand with sufficient force.

Ideally we'd like the hand to have a high a payload capability, without compromising the bandwidth of the arm, and to have a high bandwidth without too large a transmission ratio. But first we need to have a better understanding of how the bandwidths of the two systems are related.

---

* This would seem to suggest that we want to make the system as stiff as possible except that in some cases, a compliant system is more stable under force control [Whitney, 87]. [Townsend, 88] explains in greater detail the tradeoffs between mechanical bandwidth and the compliance.

2.1.1 WAM and WAM hand/wrist Mechanical Bandwidth

As in [Townsend, 88], we can model both the arm, and the hand/wrist assembly as an inertia, J_l, driven by a transmission with some transmission ratio, N, and transmission stiffnesses K_{tr} and a contact stiffness K_c (shown in Figure 2.1.1).

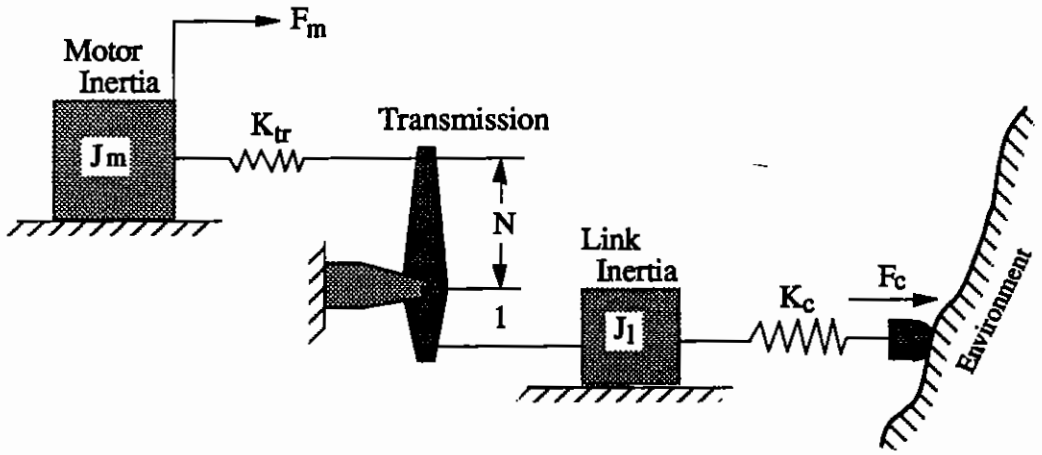

Figure 2.1.1. Model of the Robot with Motor and Link Inertia, Transmission and Contact Stiffness

The force transfer function of this simple approximation of the system is

$$\frac{F_c}{F_m}(s) = \frac{K_{tr}K_c}{J_mJ_ls^4 + (J_mK_c + J_lK_{tr} + N^2J_mK_{tr})s^2 + K_{tr}K_c} \qquad (2.1.1)$$

In this system, there is a breakpoint in the frequency response beyond which additional transmission stiffness will no longer increase the response. For low transmission ratios, this point occurs when the the transmission stiffness is equal to the impedance matched load and actuator,

$$K_{tr} = K_c\frac{J_m}{J_l} \ . \qquad (2.1.2)$$

This point is suggested by Townsend to be the optimum stiffness because it will produce the best mechanical response while still maintaining a "reasonable" contact compliance. If we assume we can create a system with the optimum transmission stiffness, the maximum frequency will be on the order of

$$\omega \approx \sqrt{\frac{K_c}{J_l}} \qquad (2.1.3)$$

Both the WAM and the WAM hand/wrist can be approximated using this model, and from equation (2.3) we can see that the mechanical bandwidth of the arm is inversely proportional to the link inertia, and by minimizing the inertia we will maximize the bandwidth.

The design decisions cannot be made solely on bandwidth, however, because speed is a more difficult (and perhaps important) performance requirement to meet. Therefore, we can attempt to keep the inertia of the hand and wrist as low as possible, assume we want to place the actuators as far back in the forearm as we can, and then add a covering to the hand contact surfaces to bring it to the optimum bandwidth. Once we have made this decision, there are many different sensors which can be added to improve the performance.

2.1.2 Sensors, Feedback Loops and Closed-loop bandwidth

A typical closed-loop force control algorithm requires measuring the force at some location and modifying the motor torque accordingly. For the kind of high bandwith force control that the WAM and the WAM wrist/hand are designed to employ, rapidly measuring and controlling the contact forces between the hand and the environment is desirable. Most sensors, however, can only respond quickly to disturbances that they are colocated with, and the further away the sensors are from the disturbance, the lower their response

bandwidth. The following are a few of the possible sensor types considered for the hand and actuators:

Tip sensors, such as the [Bicchi, 90] fingertips, have the highest precision because they are measuring the robot's contact forces directly. For dextrous manipulation, this precision is necessary because the contact between the robot, and the environment being manipulated, must be constantly monitored [Brock, 87]. However, with fingertip sensing there is a lag between any force disturbance at the actuator (such as torque ripple) and the fingertip sensor sensing it. This limits the bandwidth of the closed loop system and can lead to contact instabilities [Whitney, 87].

Locating torque sensors at each joint is another method of measuring hand forces. The joints are closer to the actuators than the fingertip sensors (increasing the force bandwidth somewhat), but this sensing strategy has compromised endpoint precision since the end effector contact forces must be calculated from joint torques, a process which is subject to modeling errors.

Monitoring the actuator current (Amps or fluid flow and pressure), and inferring the hand forces is a simple, fast, low weight, low complexity, open-loop method for effecting force control. This is the least accurate method for calculating contact forces, unless very low friction transmissions are used (as in the WAM). Also, pure current control does not compensate for torque ripple or other internal losses in the actuator.

One method for achieving better actuator current torque control is to have a torque or force sensor right on the actuator [Levin, 90]. This sensor may be used to close a control loop around the actuator, enclosing the non-linear actuator losses. There is still the problem, however, of the potentially low-precision contact force sensing if the transmission is not very efficient.

The most accurate high bandwidth control loop is a combination of a tight, fast inner control loop (enclosing all of the non-linear actuator losses), and a precise outer sensor loop.

2.2 Backdriveability

Backdriveability is a measure of how much force is required to drive the actuator from forces applied to the manipulator. It is desirable to have high backdriveability for high bandwidth force control, since such a manipulator will respond to impulse forces more rapidly, and more accurate force information can be read from the actuator control loop. [Townsend, 88] discusses two manipulator attributes, inertia and friction, that limit backdriveability.

The inertia in the manipulator links and in the actuator (as seen through the transmission) resist forces applied to the manipulator. This effect can by minimized by having low-mass links and actuators with low-mass moving parts (i.e. a motor's rotor or a pneumatic cylinder's piston). The low mass actuators become even more important if the transmission ratio (N) is high, as the effective inertia of the rotor or piston is increased by N^2.

Friction (viscous and coulomb) in the manipulator joints and transmission will also resist externally applied forces. This effect can be minimized by avoiding high-friction transmission elements such as lead screws, worm gears, and harmonic drives.

2.3 Speed and Inertia Tradeoffs

Given a limited torque capability in each of the joints of the WAM, any additional link mass (in the form of an actuator package) will increase the rotational inertia of the link and will decrease the available acceleration. We can minimize some of the effects of the increased mass if we can concentrate it further back in the arm (decreasing the added rotational inertia which is of the form ml^2), but, if we use cable to control the hand, there is more compliance in the transmission when the actuators are further away from the hand/wrist. We need to find a compromise that minimizes rotational inertia of the last link

and retains some of the desirable proximity of the actuator package to the hand/wrist (for bandwidth considerations).

In this section I will model the current acceleration capabilities of the WAM and compare them to predicted capabilities with the retrofitted hand/wrist. I will then use this model to estimate the effect of the actuator package on the ability of the WAM to complete various tasks.

Cartesian endpoint acceleration was chosen for the comparison because it is the limiting factor in trajectory speeds.

2.3.1 The current dynamics of the WAM

Rather than use the complete set of equations of motion for the WAM (which are complex and highly coupled), I chose to examine acceleration from rest in one plane of the WAM's workspace (shown in Figure 2.3.1). This subset of the workspace is reasonably

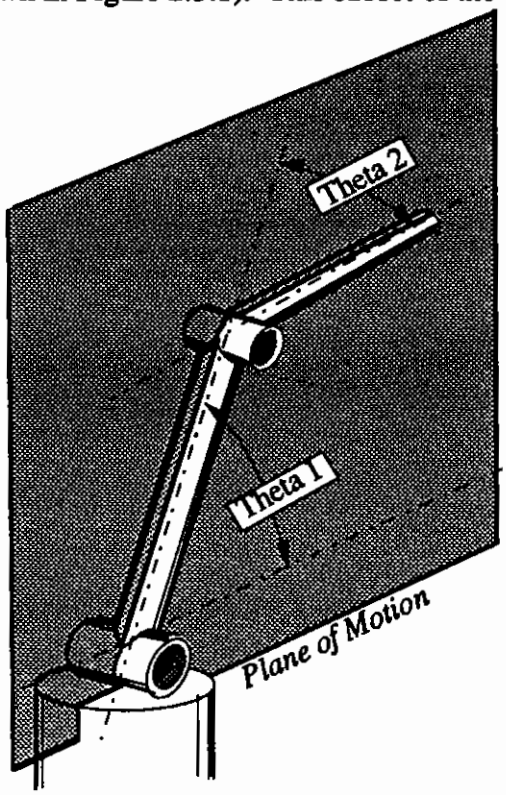

Figure 2.3.1 WAM Plane of Motion to be Modeled.

representative of the remaining workspace, and can be used to make a preliminary assessment of the effects of increased mass on the WAM. In addition, modeling acceleration from rest lets us drop the Coriolis force terms, simplifying the equations while still keeping a valid basis for comparison.

The Equations of Motion

Throughout this next section I will be using methods and nomenclature from [Craig, 86] which is an excellent reference for robot dynamics. The procedure I used for finding the maximum accelerations available was: 1) determine the joint accelerations required for producing Cartesian acceleration in the desired direction, 2) determine the torque required at each joint to produce those joint accelerations, and 3) apply the joint torque limits to the combined expressions 1) and 2), to find the endpoint's maximum Cartesian acceleration.

Finding the Joint Accelerations

In order to find the endpoint accelerations for the WAM, we need the Jacobian matrix which maps joint velocities to endpoint velocities:

$$V = J\dot{\Theta}. \qquad (2.3.1)$$

In the chosen subset of the WAM's workspace, the WAM can be modeled as a simple planar, revolute manipulator for which the Jacobian is:

$$\begin{bmatrix} v_x \\ v_y \end{bmatrix} = \begin{bmatrix} -L_1 sin(\Theta_1) - L_2 sin(\Theta_1+\Theta_2) & -L_2 sin(\Theta_1+\Theta_2) \\ L_1 cos(\Theta_1) + L_2 cos(\Theta_1+\Theta_2) & L_2 cos(\Theta_1+\Theta_2) \end{bmatrix} \begin{bmatrix} \dot{\Theta}_1 \\ \dot{\Theta}_2 \end{bmatrix} \qquad (2.3.2)$$

To find the endpoint acceleration, we need to take the derivative of equation 2.3.1,

$$\dot{V} = \dot{J}\dot{\Theta} + J\ddot{\Theta} \qquad (2.3.3)$$

but, if we look only at acceleration from rest of the end effector for a given position, then $\dot{\Theta} = 0$, and the Jacobian provides the linear mapping from joint acceleration to endpoint acceleration:

$$\dot{V} = J\ddot{\Theta} \qquad (2.3.4)$$

$$\begin{bmatrix} a_x \\ a_y \end{bmatrix} = \begin{bmatrix} -L_1 sin(\Theta_1) - L_2 sin(\Theta_1+\Theta_2) & -L_2 sin(\Theta_1+\Theta_2) \\ L_1 cos(\Theta_1) + L_2 cos(\Theta_1+\Theta_2) & L_2 cos(\Theta_1+\Theta_2) \end{bmatrix} \begin{bmatrix} \ddot{\Theta}_1 \\ \ddot{\Theta}_2 \end{bmatrix} \qquad (2.3.5)$$

Solving equation 2.3.5 for $\ddot{\Theta}_1$ and $\ddot{\Theta}_2$, we find the necessary joint accelerations to produce a desired endpoint acceleration a_x, a_y:

$$\ddot{\Theta}_1 = \frac{-(a_x cos(\Theta_1+\Theta_2) + a_y sin(\Theta_1+\Theta_2))}{(L_1(sin(\Theta_1)cos(\Theta_1+\Theta_2) - cos(\Theta_1) sin(\Theta_1+\Theta_2)))} \qquad (2.3.6)$$

$$\ddot{\Theta}_2 = \frac{(a_x L_1 cos(\Theta_1) + a_y L_1 sin(\Theta_1) + a_x L_2 cos(\Theta_1+\Theta_2) + a_y L_2 sin(\Theta_1+\Theta_2))}{(L_1 L_2(sin(\Theta_1)cos(\Theta_1+\Theta_2) - cos(\Theta_1)sin(\Theta_1+\Theta_2)))} \qquad (2.3.7)$$

this can also be expressed as:

$$\ddot{\Theta} = J^{-1}\dot{V} \qquad (2.3.8)$$

where J^{-1} is the inverse Jacobian matrix.

We can set these expressions aside while we find the joint torques as a function of the joint accelerations.

Finding Joint Torques

The torque required at the centroid of each link to produce an angular acceleration is:

$$T_1 = I_{cm1}(\ddot{\Theta}_1) \qquad (2.3.9)$$

$$T_2 = I_{cm2}(\ddot{\Theta}_2) \qquad (2.3.10)$$

There is, however, coupling between the two links as the links are being accelerated while in contact with each other. Also, the torques are not being applied at the center of mass, but at the joints. Figure 2.3.2 shows free-body diagrams of the links and the interactions between them.

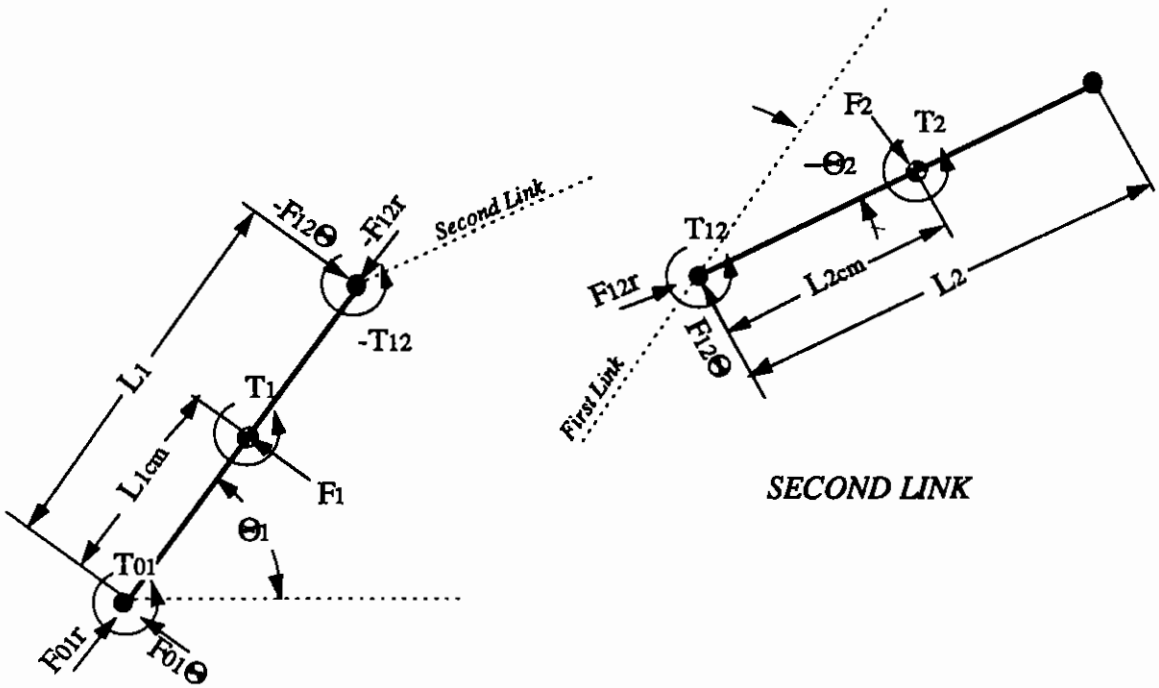

Figure 2.3.2. Free Body Diagram of the Planar revolute robot.

In this case, the body forces are a result of the linear acceleration of the centroid:

$$F_1 = m_1(\ddot{r}_1) \qquad (2.3.11)$$
$$F_2 = m_2(\ddot{r}_2) \qquad (2.3.12)$$

so the forces exerted at each of the joints ($F_{01}\,\hat{r} + F_{01}\,\hat{\Theta}$) are

$$F_{01} = m_1(\ddot{r}_1) + F_{12} \qquad (2.3.13)$$
$$F_{12} = m_2(\ddot{r}_2). \qquad (2.3.14)$$

The expressions for the coupled torques on each member (from [Craig, 89]) are:

$$T_1 = T_{01} - T_{12} + L_{cm1} \times F_{01} + (L_1 - L_{cm1}) \times F_{12} \qquad (2.3.15)$$

$$T_2 = T_{12} + L_{cm2} \times F_{12} \qquad (2.3.16)$$

By expanding the cross products, and solving equations (2.3.15 and 2.3.16) for the torques at the joints (T_{01} and T_{12}), we can find the coupled joint torques:

$$T_{01} = (I_{cm1} + m_1 L_{cm1}^2 + L_1 L_{cm2} m_2 \cos(\Theta_2) + m_2 L_1^2)(\ddot{\Theta}_1) + (L_{cm2} m_2 L_1 \cos(\Theta_2) + I_{cm2} + m_2 L_{cm2}^2)(\ddot{\Theta}_1 + \ddot{\Theta}_2) - m_2 L_1 L_{cm2} \sin(\Theta_2)\dot{\Theta}_2^2 + m_2 L_{cm2} g \cos(\Theta_1 + \Theta_2) + m_1 g \cos(\Theta_1)(L_{cm1} + L_1) \qquad (2.3.17)$$

$$T_{12} = (I_{cm2} + m_2 L_{cm2}^2)(\ddot{\Theta}_1 + \ddot{\Theta}_2) + L_1 L_{cm2} m_2 \cos(\Theta_2)(\ddot{\Theta}_1) - m_2 L_1 L_{cm2} \sin(\Theta_2)\dot{\Theta}_2^2 + m_2 L_{cm2} g \cos(\Theta_1 + \Theta_2). \qquad (2.3.18)$$

We can pull out the gravity terms (T_{g1} and T_{g2}) since (for a given Θ) they will act as a constant bias torque on the joint actuators and can simply be subtracted from the joint torque limits:

$$T_{g1} = m_2 L_{cm2} g \cos(\Theta_1 + \Theta_2) + m_1 g \cos(\Theta_1)(L_{cm1} + L_1) \qquad (2.3.19)$$

$$T_{g2} = m_2 L_{cm2} g \cos(\Theta_1 + \Theta_2) \qquad (2.3.20)$$

and, since we are accelerating from rest, all of the velocity terms become zero leaving us with actuator torque as a function of joint accelerations:

$$T_{01} = (I_{cm1} + m_1 L_{cm1}^2 + L_1 L_{cm2} m_2 \cos(\Theta_2) + m_2 L_1^2)(\ddot{\Theta}_1) + (L_{cm2} m_2 L_1 \cos(\Theta_2) + I_{cm2} + m_2 L_{cm2}^2)(\ddot{\Theta}_1 + \ddot{\Theta}_2) \qquad (2.3.21)$$

$$T_{12} = (I_{cm2} + m_2 L_{cm2}^2)(\ddot{\Theta}_1 + \ddot{\Theta}_2) + L_1 L_{cm2} m_2 \cos(\Theta_2)(\ddot{\Theta}_1). \qquad (2.3.22)$$

In matrix form, these torques can be expressed as:

$$T = I\ddot{\Theta} \qquad (2.3.23)$$

where I is the inertia matrix for the manipulator. Substituting for $\ddot{\Theta}$ using equation 2.3.8, we get

$$T = IJ^{-1}\dot{V} \qquad (2.3.24)$$

The expanded form of equation 2.3.24 gives us the mapping of joint torques to endpoint accelerations, (including the ratio of the two joint torques for a given acceleration direction). Using it, we can find the maximum acceleration that still satisfies constraint of the joint torque limits. However, we don't have the complete expression yet. We still need to find the position of the centroid (L_{cm}) and the inertia about the centroid (I_{cm}) for each link. Once we have the L_{cm} and I_{cm}, we will be able to evaluate the expression for the torques in each manipulator configuration, and be able to find the acceleration limits.

Finding the I_{cm} and L_{cm} of Each link

Since neither of the links have evenly distributed mass, we must use the parallel axis theorem (equation 2.3.25) to determine both the inertias about the centers of mass I_{cm1} and I_{cm2}, and their inertias about joints 1 and 2 (I_1, I_2). The parallel axis theorem states that the moment of inertia of any body rotating about a point P is equal to the mass of the body times the square of the distance to the centroid (L_{cm}), plus the body's moment of inertia about that centroid (I_{cm}):

$$I_P = (\Sigma masses)\,(L_{cm})^2 + I_{cm}. \qquad (2.3.25)$$

The first link:

I modeled the first link as a hollow cylinder of mass M_{T1}, radius r_{T1}, length L_1, and a center of mass at $^1/_2\,L_1$, and the elbow joint as a sphere of mass M_E and radius r_E at a distance L_1 from the base (see Figure 2.3.3).

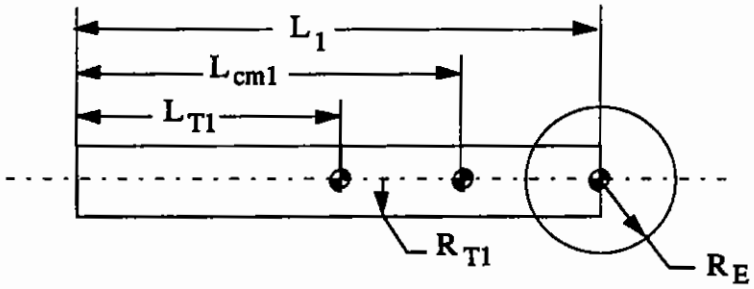

Figure 2.3.3. Model of the first Link

Using equation (2.3.25) the inertia I_1 of the link as a function of M_{T1}, M_E, and L_{cm1} is:

$$I_1 = (M_{T1} + M_E)L_{cm1}^2 + I_{cm1}. \qquad (2.3.26)$$

Using the expressions for moments of inertia of a sphere

$$I_{cmS} = {}^2/_5\, M_S(r_S)^2 \qquad (2.3.27)$$

and the moment of inertia of a thin-walled tube about its transverse axis

$$I_{cmT} = M_T{}^1/_{12}(6r_T^2 + L_T^2) \qquad (2.3.28)$$

where r_{TI} is the outer radius of the tube, the I_{cm} of the first link as a function of M_{T1}, M_E, L_{cm1}, L_1, r_{T1}, and r_E is:

$$I_{cm1} = M_{T1}[(L_{cm1} - {}^1/_2 L_1)^2 + {}^1/_{12}(6r_{T1}^2 + L_1^2)] + M_E[(L_1 - L_{cm1})^2 + {}^2/_5 (r_E)^2] \qquad (2.3.29)$$

and L_{cm1}, the position of the centroid, is equal to :

$$L_{cm1} = \frac{L_1 (M_{T1} + 2M_E)}{2 (M_{T1} + M_E)}, \qquad (2.3.30)$$

The second link:

I modeled the second link as a long hollow cylinder of mass M_{T2}, radius r_{T2} and length L_2 with a center of mass at ${}^1/_2 L_2$; the hand as a sphere (a very rough approximation) of radius r_H and mass M_H at the end of the arm (L_2 in from the axis of rotation in the elbow); and the actuator package as a cylinder (an estimate) with radius r_A, length l_A, and mass M_A at distance L_A from the same axis of rotation (see Figure 2.3.4).

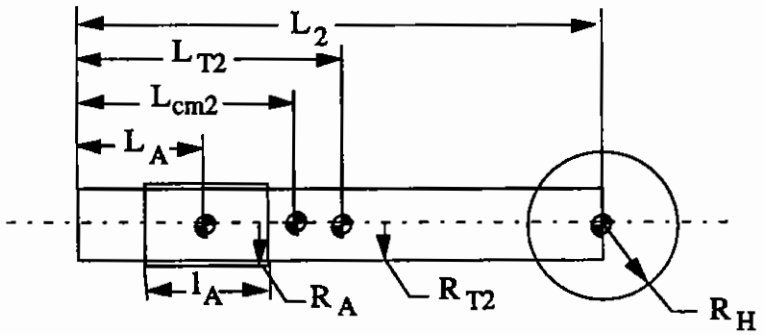

Figure 2.3.4. Model of the Second Link

Again, using equation (2.3.25), the inertia about the elbow joint can be expressed as:

$$I_2 = (M_{T2} + M_A + M_H)L_{cm2}^2 + I_{cm2} \qquad (2.3.31)$$

Using equations, 2.3.27 and 2.3.28, and the moment of inertia of a cylinder about its transverse axis:

$$I_{cmT} = M_T {}^1/_{12}(3r_T^2 + L_T^2) \qquad (2.3.32)$$

I_{cm2} can be approximated as a function of M_A, M_H, M_{T2}, L_A, L_2, l_A, r_A, r_H, and r_{T2}.

$$I_{cm2} = M_A[L_A^2 + {}^1/_{12}(3r_A^2 + l_A^2)] + M_H[L_2^2 + {}^2/_5 (r_H)^2] + M_{T2}[({}^1/_2 L_2)^2 + {}^1/_{12}(6r_{T2}^2 + L_2^2)] \qquad (2.3.33)$$

where L_{cm2} is :

$$L_{cm2} = \frac{(2L_A M_A + 2L_2 M_H + L_2 M_{T2})}{(2 (M_A + M_H + M_{T2}))} \qquad (2.3.34)$$

Note this applies to the current WAM as well, because setting the value of M_A to zero gives us the I_{cm2} of the current forearm without the actuator package.

After including the parameter values for the WAM (given in Table 2.3.1), and solving with the estimated limits (3 lbm. actuator package with a centroid at 5" and 10"), the link inertias, I_{cm1} and I_{cm2}, about their centroids become:

I_1 = .05166 ft-lbs-sec^2 (Does not change)
I_2 = .00895 ft-lbs-sec^2 (Old hand, no actuator package)
I_2 = .01994 ft-lbs-sec^2 (New hand, 3 lbm package at 5")
I_2 = .0108 ft-lbs-sec^2 (New hand, 3 lbm package at 10")

Parameter	Symbol	Value	[Metric]
Pitch Torque Limit	T_1	900 in-lbs	[102 Nm]
First Link Length	L_1	22.5 "	[.560 m]
First Link Radius	r_{T1}	1.5"	[.038m]
First Link Mass	M_{T1}	1.9 lbm.	[.862 Kg]
Elbow Mass	M_E	3.1 lbm.	[1.4 Kg]
Elbow Radius	r_E	2.5 "	[.064m]
Elbow Torque Limit	T_2	285 in-lbs	[32 Nm]
Second Link Length	L_2	14"	[.350 m]
Second Link Radius	r_{T2}	1"	[25.6 mm]
Second Link Mass	M_{T2}	1 lbm.	[.4545 kg]
Hand Mass (currently)	M_H	.9 lbm	[.408 Kg]
Estimated Parameters	**Symbol**	**Value**	**[Metric]**
Hand Mass (new)	M_H	1.2 lbm	[.545 Kg]
Hand Radius	r_H	2.5"	[.064m]
Actuator Package Length	l_A	6"	[.152 m]
Actuator Package Radius	r_A	1.25"	[.032 m]
Variables	**Symbol**	**Value**	**[Metric]**
Actuator Package Mass	M_A	0 - 3 lbm	[1.36 Kg]
Hand Mass	MH	.9 - 1.2 lbm	[.41 - .545 Kg]
Actuator Distance from Elbow	L_A	5" - 10"	[.128 - .256m]

Table 2.3.1 WAM and Hand/Wrist Parameters used for Model

Note that the inertia about the centroid is lower for the forearm with the actuator package further out on the arm because the weight is nearer the centroid, this is offset in link inertia about the endpoint, by the more distant centroid.

Entering the parameter values from Table 2.3.1 into equations 2.3.21 and 2.3.22 and adding the expressions for the inertias (equation 2.3.29 and 2.3.33), the torques become:

$$T_{01} = .7165\ \ddot{\theta}_1 + .1485\ (\ddot{\theta}_1 + \ddot{\theta}_2)$$ ft-lbs (Old hand, no actuator package)

$$T_{01} = 1.1727\ \ddot{\theta}_1 + .2721\ (\ddot{\theta}_1 + \ddot{\theta}_2)$$ ft-lbs (New hand, 3 lbm package at 5")

$$T_{01} = 1.2459\ \ddot{\theta}_1 + .3941\ (\ddot{\theta}_1 + \ddot{\theta}_2)$$ ft-lbs (New hand, 3 lbm package at 10")

$$T_{12} = .0957\ \ddot{\theta}_1 + .0528(\ddot{\theta}_1 + \ddot{\theta}_2)$$ ft-lbs (Old hand, no actuator package)

$$T_{12} = .1893\ \ddot{\theta}_1 + .0828(\ddot{\theta}_1 + \ddot{\theta}_2)$$ ft-lbs (New hand, 3 lbm package at 5")

$$T_{12} = .2625\ \ddot{\theta}_1 + .1316(\ddot{\theta}_1 + \ddot{\theta}_2)$$ ft-lbs (New hand, 3 lbm package at 10")

Finding Acceleration capability

Combining these with the acceleration Jacobian (equation 2.3.24), the torque limits, and the gravity torques we can determine the maximum endpoint acceleration capability of the WAM as a function of endpoint position and acceleration direction. Gravity produces an offset in the torque limits for each position, but because the arm is capable of very large accelerations, the difference between the acceleration capability with and without gravity is very slight (see Figure 2.3.5)

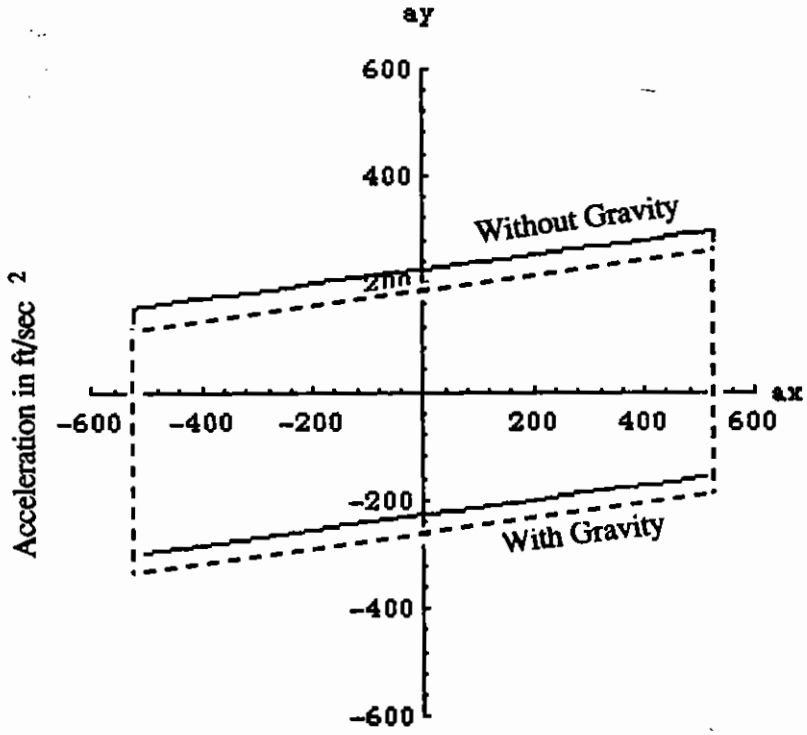

Figure 2.3.5. The Effect of Gravity on Acceleration of the WAM.First link Horizontal, 90º Between Links.

Figure 2.3.6. shows the results from the simulation. At each endpoint position of the WAM, there are superimposed polar plots of maximum attainable acceleration

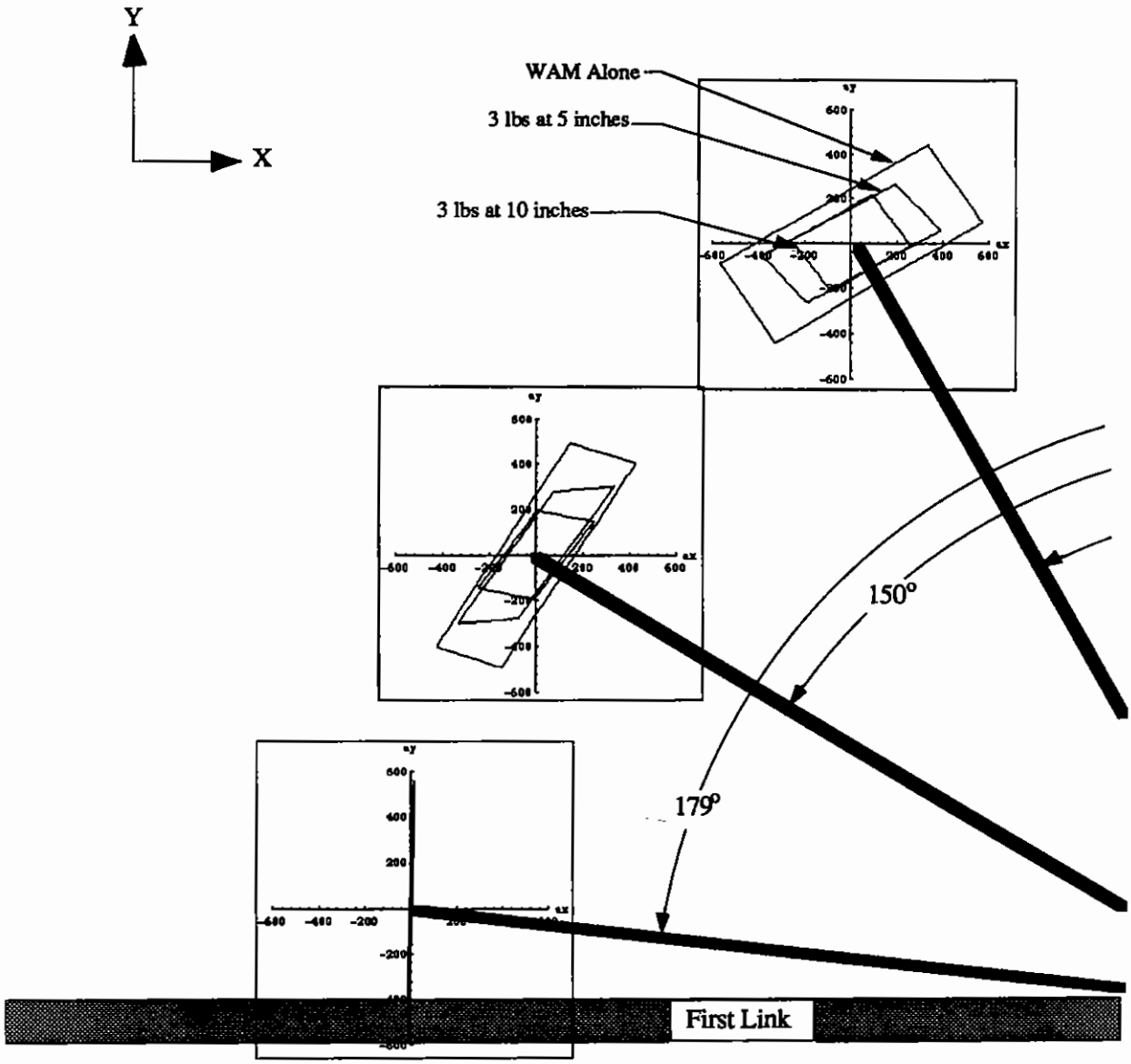

Figure 2.3.6. Acceleration Capability (in ft/sec^2) of the WAM in Seven Configurations

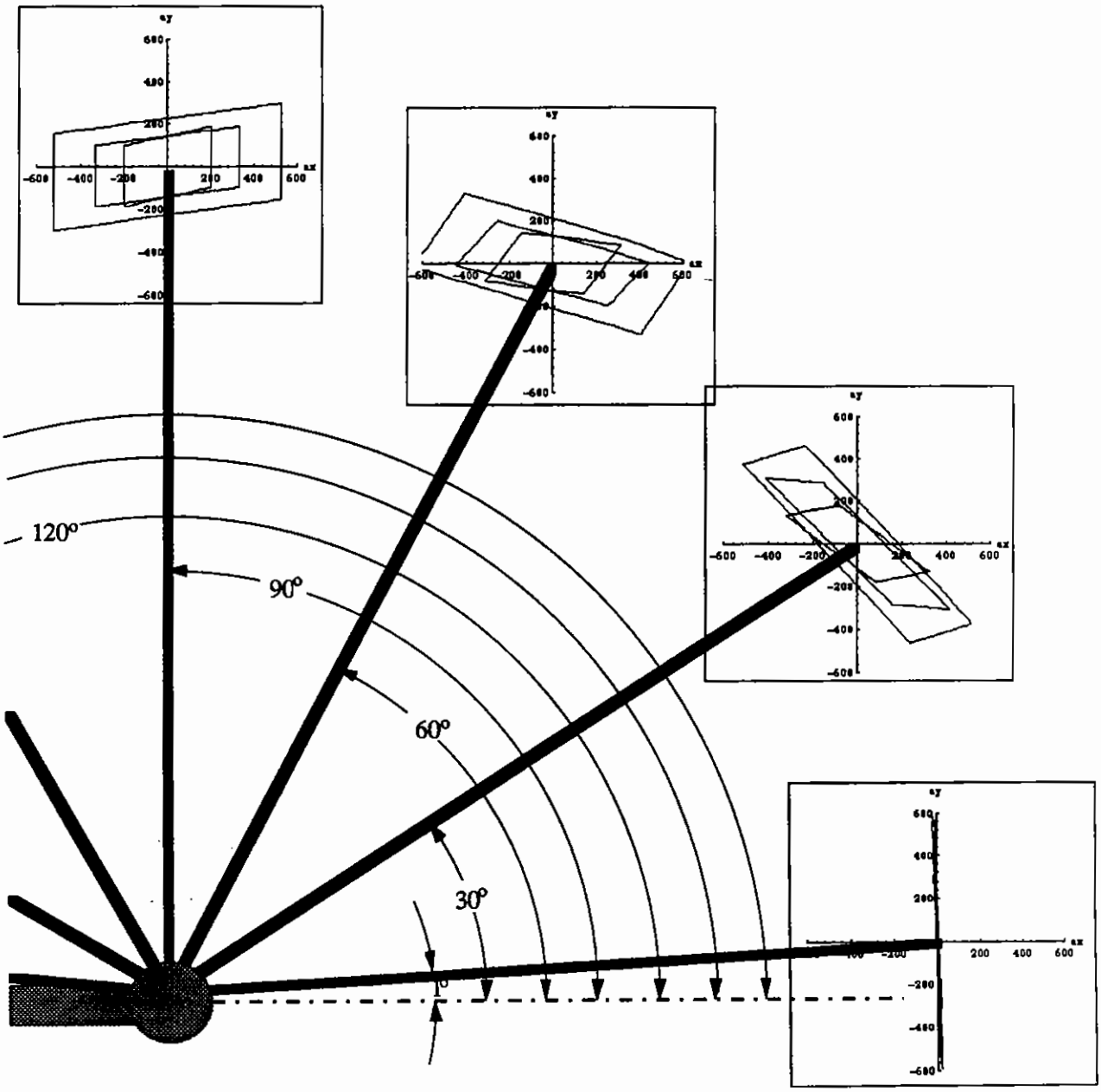
120°
90°
60°
30°
0°

(neglecting gravity) for the three cases looked at before: the current WAM configuration without an actuator package mass, and the 3 lbm. actuator package placed at five inches and at ten inches from the elbow. The angles shown are 1°, 30°, 60°, 90°, 120°, 150°, and 179°.

As we would expect, when the "actuator package" is added to the arm, the overall maximum acceleration is decreased. Also from Figure 2.3.6 we can see that the torque limits on the joints produce a semi-rectangular acceleration "envelope" and this envelope is skewed slightly as weight is added to different spots on the forearm, changing the center of mass. The different centroids have this effect since, for all motions, the link is pivoting about some point in space (the instantaneous center of rotation). This, in some cases, will cause the effective inertia of the link with the actuator package at 10" seem smaller in some cases than it does with the gearbox at 5" (when the instantaneous center is closer to the centroid of the link).

The trade-off boils down to choosing between a fast responsive arm, a fast responsive hand, or an appropriate compromise between the two.

2.3.2 What this means for the design

Since the hand's placement is naturally at the end of the arm, and the size and shape are already fixed, the best way to maintain arm dynamics is to make the hand as light as possible. In the actuator package, however, it is often difficult to reduce the weight of individual "off the shelf" actuators. Fortunately, the size, shape and position may be chosen to minimize inertia. From equation (2.3.31) and Figure 2.3.6 we can see that the inertia will increase as the actuator package is placed further from the joint. Although motion trajectories may be planned to maximize the acceleration capability of the WAM along that path, without depending on the controller to work around mechanical deficiencies in the robot, the best actuator package is (not too surprisingly) as compact and

light as possible, and as close to the elbow as possible. There are however, many other requirements that the hand/wrist must meet. In the next Chapter, System Specifications, the full set of design requirements will be developed.

3.0 System Specifications

There were many different design constraints which needed to be satisfied when designing the actuator package for the hand. Since the hand had already been designed to be actuated with cable tendons, the actuators must either pull the cables linearly like muscles and pneumatic cylinders, or wrap the cable onto a capstan. Also as we saw in Section 2.1, the hand/actuator package also needed to be light enough to avoid compromising the performance of the arm while strong enough to accomplish the set tasks.

This chapter examines all the requirements that the actuator package was subject to. Any "hard number" specifications (as opposed to guidelines) are boxed.

3.1 Size

The actuator package and hand were to be retrofitted onto the existing WAM. The nature of the WAM requires it to have continuous smooth reaction surfaces [Townsend, 88] [Eberman, 89], so there could be no gross distortion of the forearm to accommodate the actuators. Most important for the WAM's manipulation capabilities are the areas on the "inside" of the arm which act as the gripping surface. This required that the thickness of the forearm in the plane of elbow movement remain at 2" so that the WAM can fully "close" (see Figure 3.1.1).

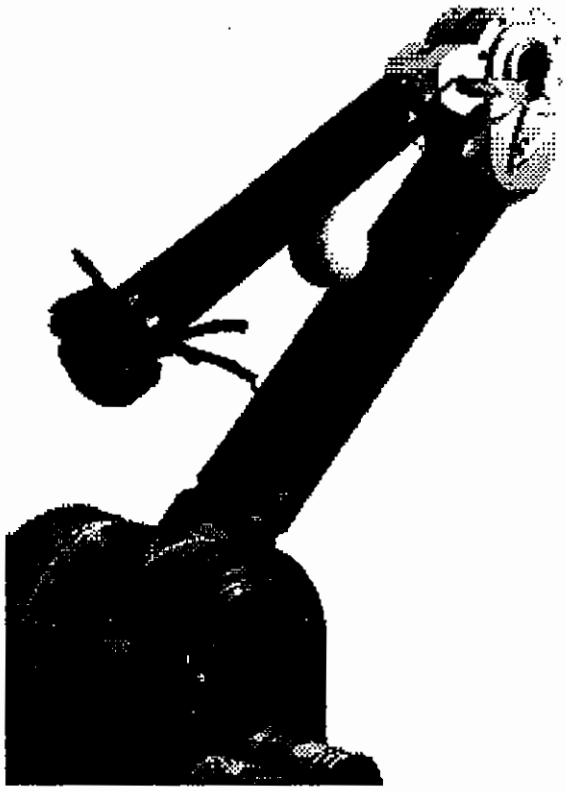

Figure 3.1.1. The WAM Gripping a Ball with the Inner Reaction Surface

3.2 number of actuators

The WAM hand has 2 DOF in the fingers and 3 DOF (roll-pitch-yaw) [Moyer, 92] in the wrist. The cabling is $n+1$ for the fingers and two axes of the wrist, and a pretensioned $2n$ design for the roll axis of the wrist. In this configuration, seven tendons are required to move the hand. However, since the two tendons for the $2n$ section of the wrist would be coupled (one would pay out exactly the same amount as was reeled in on the other), both tendons could be actuated by one motor if configured appropriately. The final specification was a minimum of six actuators, seven, if one could not do run two cables.

3.3 Gripper Speed and Acceleration

In order to catch and throw objects, the hand needs to be able to open and close in about 150ms. From the design of the hand [Moyer, 92] the maximum length of cable needed to be moved in this time is 6 in [.154 m]. In the worst case configuration of the hand and wrist, it would be one cable supplying most of the force for motion. Therefore, the final design needed to be able to pull in or pay out cable at a rate or 40 in/s (~1 m/s) under load of the inertia of the hand which was estimated to be .056 oz-in-sec^2. We can translate this into an effective mass (see Figure 3.3.1) being pulled upon linearly by the cable using the pulley radius of the first joint:

$$Effective\ M\ (slugs) = \frac{Inertia\ (oz\text{-}in\text{-}s^2)}{(pulley\ radius)^2\ (in^2)}\left(\frac{4}{3}\right) \qquad (3.3.1)$$

For a first joint pulley radius of .5", the effective mass is then .2987 slugs [4.3 Kg].

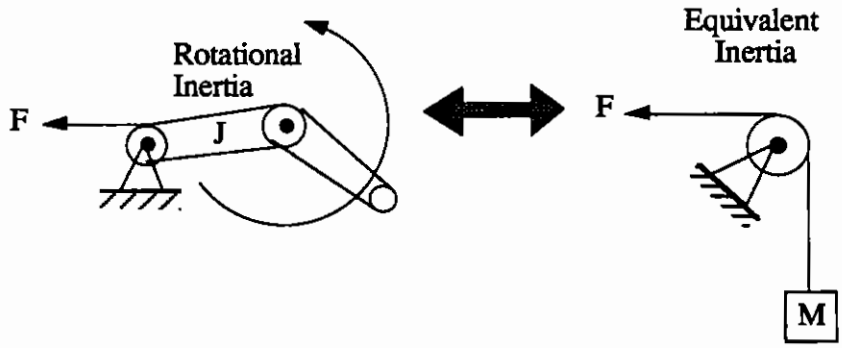

Figure 3.3.1 Equivalent Mass for a Rotational Inertia

To move this mass 6 in. in 150ms (closing the hand in 150 ms) with zero velocity at the two endpoints, we need to accelerate the hand to some velocity and then decelerate it back to zero velocity at the endpoint. Figure 3.3.2 shows several acceleration profiles which could accomplish the required task.

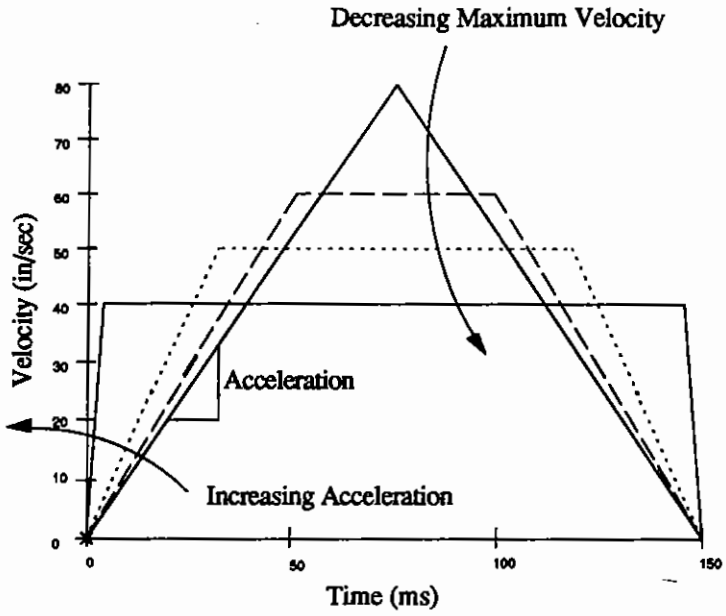

Figure. 3.3.2. Several Velocity Profiles for Moving 6 inches in 150 ms.

The minimum required acceleration to complete the task is the triangular velocity path, where the hand will be accelerating for half the time (t/2) and distance (d/2) and decelerating at the same rate for the remainder. Calculating acceleration for the first half gives us the required cable acceleration:

$$a = \frac{d}{\left(\frac{t^2}{4}\right)} = \boxed{1067\ in/sec^2\ [27.3\ m/sec^2]} \qquad (3.3.2)$$

with a cable tension of 15 lbs [67 N]

In practice this will be somewhat overdesigned because more than one cable will often be pulling on the hand, but this means that the wrist/hand will be capable of the required acceleration even when holding small objects (such as tools).

3.4 Strength and Power

There are two constraints on actuator strength: the tension needed to accelerate the hand at the required rate, and the static tension needed to grasp an object.

It was desired to make the hand capable of gripping and retaining the heaviest object the arm was expected to manipulate (the WAM was designed to be able to accelerate a 2 Kg object at 2*g* [Townsend, 88]). If the hand were to match the arm in strength, from simulations in [Moyer, 92] it was determined that the maximum load on any one cable would be 40 lbs [180 N] (see Figure 3.4.1). This 40 lb. strength would allow the hand to hold onto a 1 lb. object with a 1 lb. grip force while the object was subjected to a 2 lb. force in any direction.

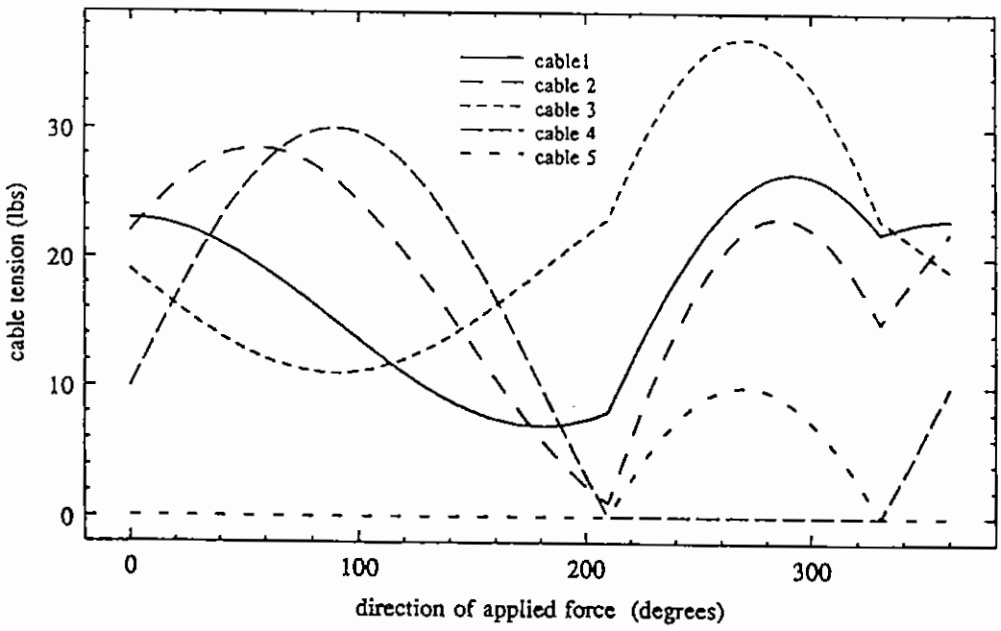

Figure 3.4.1. Tendon Tension for the Wrist/Hand Cables vs. Force Angle for the Hand Holding a 1 lb Object with a 1 lb. Grip force, Subject to a Rotating 2 lb. Force.

In addition to hanging on to objects being moved around by the WAM, the hand needs to manipulate objects. If we assume that a required manipulation task for the hand might be moving a 2 Kg object at a rate of 1m/s against gravity, and if we assume that in the worst case, one tendon is doing most of the load carrying, a single actuator must be capable of producing 20 Watts output shaft power.

3.5 Arm Speed and Hand Bandwidth

The WAM is intended for unstructured environments, so it is not surprising that performance specification were occasionally vague. Because of this, the tradeoff between bandwidth and speed between the hand and the arm is not well defined. We could run simulations to see how the arm would behave in different parts of it's workspace with the additional mass of the hand and actuators on it, but simulations can't tell us how the added mass and decreased acceleration will affect as yet unspecified tasks that the WAM might be called upon to perform.

One task that the WAM is being applied to, is catching objects. To do this, the trajectory of the object is determined using a vision system, and the arm tries to match that trajectory with the gripper. Once zero relative velocity between the object and the gripper has been achieved, the gripper can close on the object. This is very difficult to do with the old hand since it has a fixed orientation with respect to the last link, and in many parts of the workspace, gross motions of the arm are required to effect small endpoint orientation changes. As a result, the current hand can not catch objects in many parts of it's workspace, and it can only catch soft, spherical objects.

For catching tumbling, elongated objects (the desired ability of the new hand), the hand must be able to track the graspable orientation of the object as it is tumbling (on the small scale) while the WAM is following the object's centroid trajectory (on the large scale). As the objects to be caught become less compliant, the hand must be responsive

enough not to damage the object or the hand upon catching. Compliance in the tendons can help us here somewhat as can the hand's mechanical design [Greiner, 90]. The passively curling fingers [Greiner, 90 and Moyer, 92] respond to contact with an object by curling around that object. This curling motion helps achieve a very fast capturing response in the hand which makes the zero relative velocity of the previous catching strategy less important. These attributes of the new wrist/hand mean we may be able to afford to have the arm slightly more sluggish if we can adopt a different catching strategy (perhaps one that has the hand intersect the trajectory of the flying object rather than track it). This is a desirable situation, since we cannot add all the degrees of freedom we desire to the hand and wrist without some sacrifice in arm responsiveness. The effectiveness of these new catching strategies will have to be evaluated empirically, however, since they could not be tested without a 5 DOF hand/wrist, and we could not be sure how much the slowness of the arm would affect the WAM's catching ability.

With catching in mind, we decided that the speed performance was probably the most important requirement to meet. Therefore, we would design to keep the inertia of the hand and wrist as low as possible, place the actuators as far back in the forearm as we could, and then add a covering to the hand contact surfaces with sufficient compliance to bring the to the optimum bandwidth within the constraints set by the design (see Section 2.1.1).

3.6 Mass of the Forearm

We saw in section 2.3.1 how additional mass in the forearm is expected to slow the WAM down. From that simulation, the mass of the hand and actuator package was limited to 2.5 Kg [5.5 lbs] (as compared to .2 Kg [.44 lbs] for the carbon fibre forearm and .864 Kg [1.9 lbs] for the aluminum forearm with the pneumatic hand). This was deemed the upper limit for catching tasks.

3.7 Backdriveability

We wanted the hand to be "very" backdriveable, with low friction and inertia. This would be best accomplished by running the actuators direct-drive [Townsend and Salisbury, 88], if we could find an actuator capable of producing enough torque to wind cable with 40 lbs of force onto a 1/8" or larger shaft (or pull with 40 lbs.). However, the backdriveability constraint was downgraded to a "guideline" in favor of weight.

3.8 Sensor Requirements

For versatile hybrid position and force control of the hand, we need to have position and force feedback from the hand. Because of the independent curling nature of the fingers [Moyer, 92], we need to have both finger position feedback and actuator position feedback to know the hand's state and orientation.

I decided to try to incorporate into the actuator package both position and force/torque sensors. For low-level cable control I decided upon, optical encoders on motor shafts or Hall effect sensors on a piston, and for the fast force control loop, a strain gauge bridge on an actuator reaction surface. Additional hand sensors such as joint torque sensors, touch sensors, proximity detectors and microswitches could be more easily added later when required by specific tasks.

Even a small number of sensors result in a large number of data cables running down the arm of the robot. To alleviate these sorts of problems in robotics, sensor data busses for multiplexing sensor data are currently under development [Jacobsen, 90]. When available, we expect to install a data line of this type to handle much of the information traffic in the arm, and perhaps include in the forearm itself a small microprocessor for some preprocessing of the data.

3.9 Maintenance

Maintenance is an important, but often overlooked aspect of mechanical system design. Mechanical failure is an inevitable consequence of use, but if this is kept in mind as the robot is built, the system can be designed to be easily maintained and repaired. "Weak links" whether they are intentional, such as shear pins and fuses, or simply a consequence of trading off durability of a member against some other desirable property, should be identified and designed to be easily accessible. In the hand/wrist, replacement and retensioning of the cables is expected to be the most common maintenance required.

3.9.1 Replacing Tendons

In any cable driven robot the tendon cables must be easily accessible. Since the cables are subject to fatigue and wear as well as having to act as mechanical fuses when the hand is used beyond its designed load capability (such as being run into a wall or the floor), it must be possible to replace cables without disassembly of the actuator package.

For an experimental robotic application like this one, quick tendon replacement has the added advantage of making the hand a more practical test bed for several types of (steel and polymer) cable materials.

3.9.2 Retensioning Tendons

The system must either be immune to cable creep and stretch (as is the $n+1$ design), or have some method of retensioning which can be easily accomplished without disassembling any part of the system.

3.10 Summary

Essentially we wanted the actuator package to have tendon position and tension measurement, be compact, have almost no mass, while still being powerful, stiff, backdriveable, and serviceable.

4.0 Design Alternatives

This section details the decisions that were made during the design process and the methods that were employed to make them, including a process for choosing electric motors for servo applications. In addition, some of the design alternatives that were considered are also presented with comments on their applicability for slightly different applications.

4.1 Actuation Methods

Two main types of actuators were considered, Pneumatics / Hydraulics and electric motors.

4.1.1 Pneumatics

Pneumatics and hydraulics have a high available force/ actuator mass ratio which would seem to make them ideal for powering the WAM hand/wrist. They are not without problems however. Although they would make a compact bundle, the control would be complex, the bandwidth not high enough, and the bundle of tubes running up the inside of the arm would make the elbow stiff and affect the dynamics of the robot. When delivering high power through slender tubes, they either have high internal losses, or need a local accumulator to provide high flow. Both of these situations are unacceptable since we have no volume available in the forearm for an accumulator, and cannot meet the acceleration requirements with limited flow.

In addition, the environment the actuators may be called upon to operate in must be taken into consideration. If the hand is to be used in conditions with extremely low atmospheric pressure (such as space), all sealing and lubricating compounds will evaporate, leaving the pressure cylinders with leaky seals.

4.1.2 Electric Motors

Motors were chosen because they are clean and cheap. Further, they have high bandwidth and their control is well understood. Therefore, electric motors were used.

4.2 Transmissions

Since a backdriveable system is capable of responding gracefully to disturbances exceeding the closed loop bandwidth of the system, we wanted a backdriveable transmission for the kind of force control we intended to use. Possible options were a planetary gearbox if a direct drive system could not be used. Worm gears and harmonic drives were not even considered.

4.3 Configurations

4.3.1 Bundle

A bundle with a 2 inch width constraint is the simplest close packing arrangement. It makes sense to pack the actuators as densely as possible since as we showed in section 2.3.1 the center of mass of the actuator package should be as close to the axis of the elbow as possible. For long, slender (.5 in. dia to 1in. dia, 3+ in. long) motors, the minimally distorting configurations would be running the motors coaxially with the forearm. For short fat motors (1 in. dia to 2 in. dia, 1-3 in. long), running them perpendicular to the tendon travel would minimize the forearm distortion. See Figure 4.3.1 .

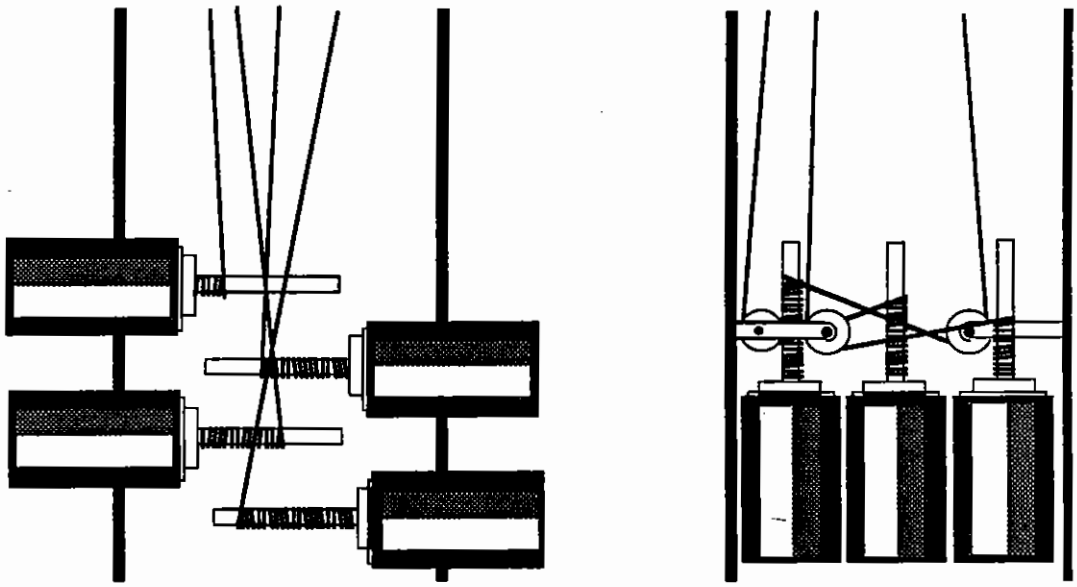

Figure 4.3.1 Perpendicular and Axial Motor Configuration

Short, slender motors may be run in either configuration, while long, fat motors would probably be too heavy to meet the design specifications, so they didn't show up in the set of possible actuators. Figure 4.3.2, shows several bundle configurations and the range of sizes for which they are applicable.

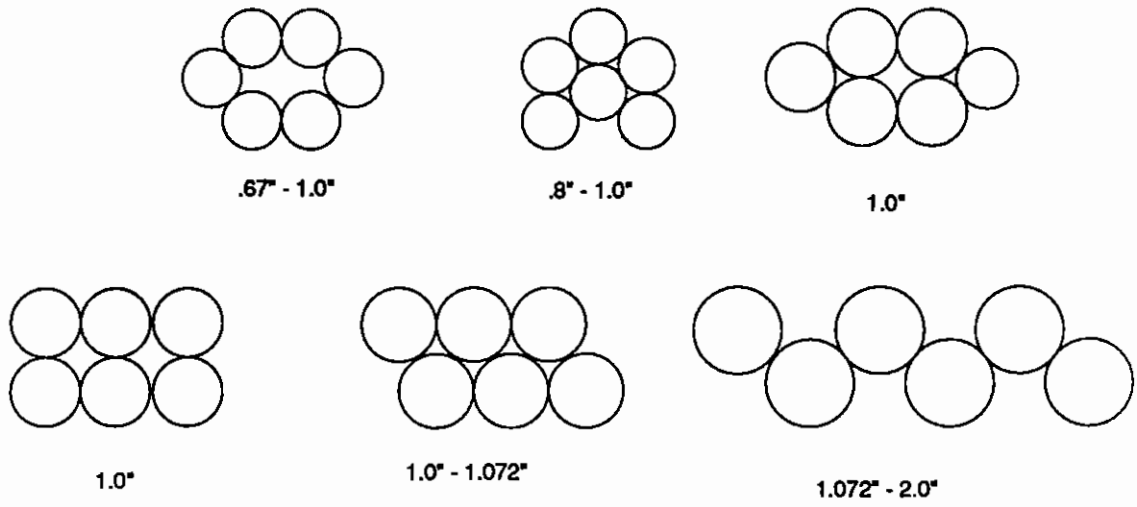

Figure 4.3.2. Different Six Actuator Bundles for Varying Sizes of Actuators.

4.3.2 Stack

There are several manufacturers of unhoused "ring" torque motors (see Figure 4.3.1).

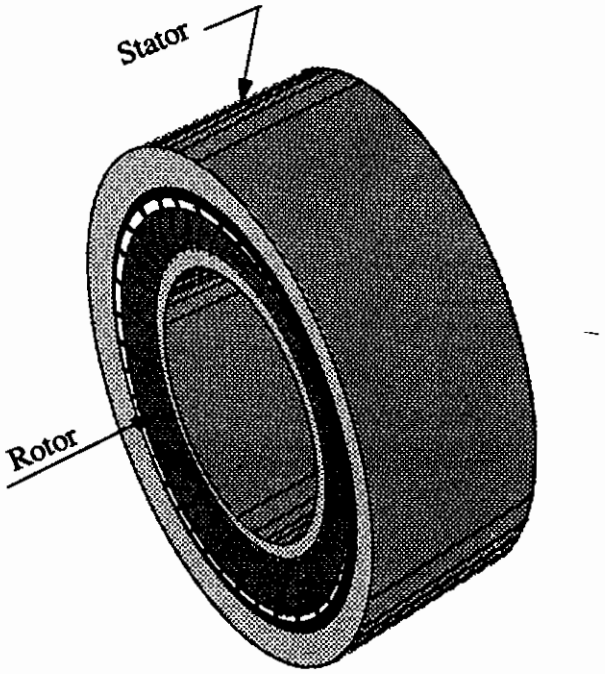

Figure 4.3.3 Ring Motor

These ring motors have the advantage of very high torque/weight ratio. This motor configuration also lends itself to running the actuator package in a "stack" configuration (see Figure 4.3.4) with the actuated tendons traveling down the center of the set of motors offset by hypoid bevel gears at different levels.

The "stack" configuration has the advantage of very low gear ratios (increasing our backdriveability), no distortion of the forearm at all, and a modular design that can be used when between 2 and 8 actuators are required.

This design, however, has a few attributes that are unsuitable for this particular application. The design requires space for a bevel gear between each motor and its neighbor. This configuration makes the actuator package very long and moves the center

of mass of the actuator package far out in the forearm (away from the elbow) which hurts the acceleration capabilities of the entire WAM. More importantly, the hypoid bevel gears, which allow us to run the capstans at different levels, gradually decrease in backdriveability as they are moved more off the central axis and become closer to high-friction worm gears. Since we needed six actuators with seven non-colliding tendons, the capstans would have to be at several different levels, and the outer cables would be much less backdriveable than the inner cables. This might not be too bad if we were running the hand with a $2n$ cabling system (some links would just be more backdriveable than other), but with the $n+1$ cabling, where each DOF is driven by a combination of actuators, uneven backdriveability could lead to very strange force control behaviors of the hand/wrist as linear external forces would produce twisting motions in the hand. Therefore, I decided to bias the motor choice towards slender conventional motors if possible.

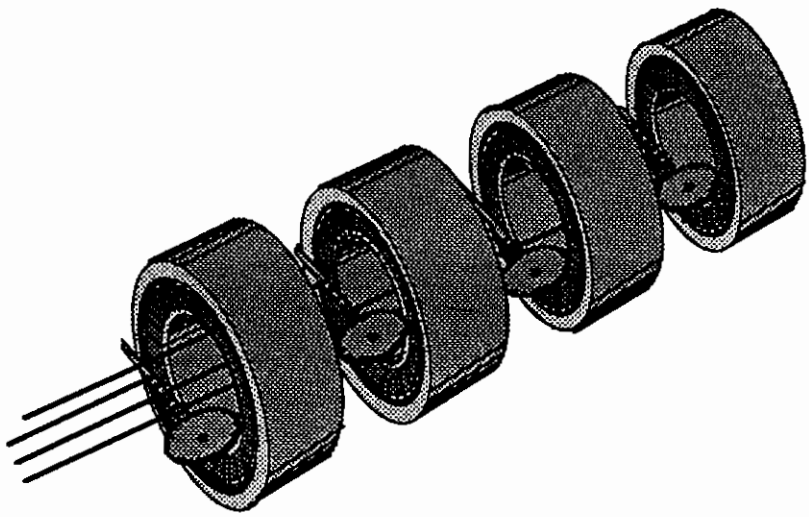

Figure 4.3.4 The Stack Configuration for Ring Motors

4.4 Bias Torques

One of the problems with pulling cables with electric motors is that one can only use half of the motor's force range since a cable can only be used in tension. A way around this would be put a constant bias torque on the motor shaft equal to the maximum continuous torque capability of the motor. The motor would then work against the bias torque to achieve zero tension on the cable and with the bias torque to achieve full tension. A motor having half the continuous stall torque rating could then be used. Advantages of this include smaller, lighter motors and constant cable tension even when there is no power in the motors (makeing less tendency to lose cables off of drive pulleys in the hand).

A convenient way of producing a constant torque on the capstan is to terminate the cable using a constant force spring* (see Figure 4.4.1).

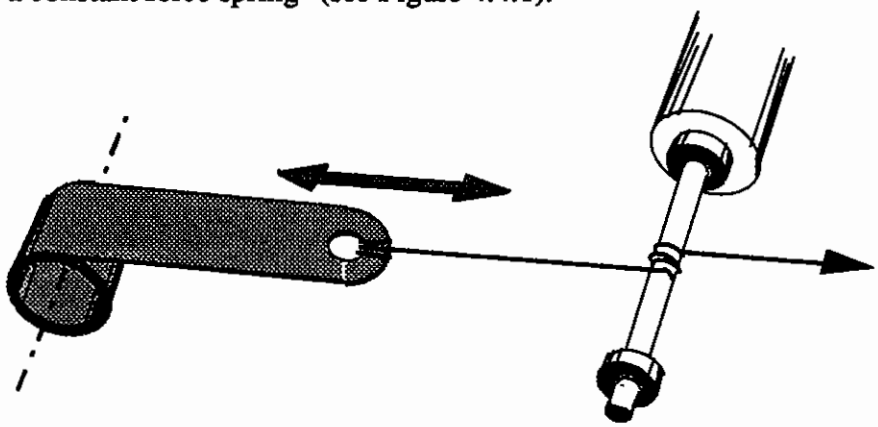

Figure 4.4.1.Bias torque using a c-force spring

The force from a "constant-force" spring is solely from the unbending of the section of spring that is coming off the spool . The force can be found using the equation

* A common linear coil spring cannot be used for this application since we need 40 lbs of force over the entire 6" of travel. If the force changes greatly as a function of shaft position, the motor must be able to supplement the coil spring over that whole range (this negates most of the power savings). However, we cannot use a linear spring with a very "flat" spring constant, since, in order to have even a 20% force change over the full cable travel, the spring would have to be 30 inches long!

$$Spring\ Force = EI\left(\frac{1}{ID^2} - \left(\frac{1}{ID} - \frac{1}{OD}\right)^2\right) \qquad (4.4.1)$$

Where E is the Modulus of Elasticity of the spring steel (typically 30x10^6 psi), ID and OD are the inner and outer diameters of the spring, and I is the moment of Inertia of the crossection ($wt^3/12$) [Sandvik].

The force/weight ratio of these springs is not terribly high for large travel distances because as the spring is unwound, the unwrapped spring material no longer adds to the force produced and just serves as heavy cable. The weight and fatigue life are the two factors determining the springs usefulness for this particular application.

To maintain sufficient life for these springs (in the case of the robot greater than 10,000 cycles)*, the springs need to have large diameters, thin crossections, and be very wide. Unfortunately, these lifetime requirements are at direct odds with maximizing the force provided and minimizing the weight and the volume taken up. The maximum fibre stress the spring will see during use [Sandvik] is taken to be

$$\sigma_{max} = E\left(\frac{t}{ID}\right) \qquad (4.4.2)$$

In order to get a cycle life of 10,000 or more, the maximum fiber stress on the upper surface of the spring must be less than 282 ksi . Unfortunately, the spring force is directly proportional to the fibre stress in the spring: the thicker the spring and smaller the inner diameter, the greater the spring force. Figure 4.4.2 shows a graph of spring force vs. spring thickness and diameter with the area of less than 10,000 cycle life indicated. The

* This is low because the cables have low cycle lives, and we can replace springs along with worn cables. Ideally, we would like the life to be much higher.

limits of the graph were chosen from the 2" design constraint, and the width of the spring was a normalized 1".

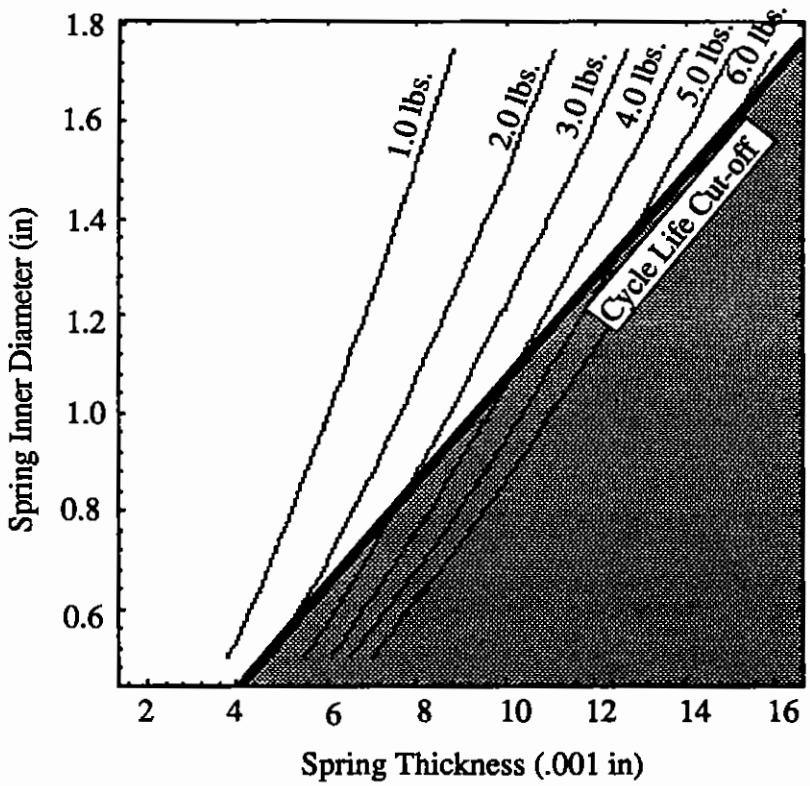

Figure 4.4.2 Spring force in lbs. vs. stock thickness and spool diameter in inches

Although life limitations restricted the use of the higher force springs, several springs can be bundled together to produce a single, higher force spring. However, we must still have a weight savings to justify using the springs, so the combined weight of the springs must be less than 5oz [.14 Kg] (half the absolute maximum weight allowed each actuator). If we take the data from spring force, determine how many of each spring would be required to produce the full 40 lbs of pull, and calculate the weight of the resultant aggregate spring, we can see in Figure 4.4.3 that the only springs which meet the weight requirements have cycle lives which are unacceptably short.

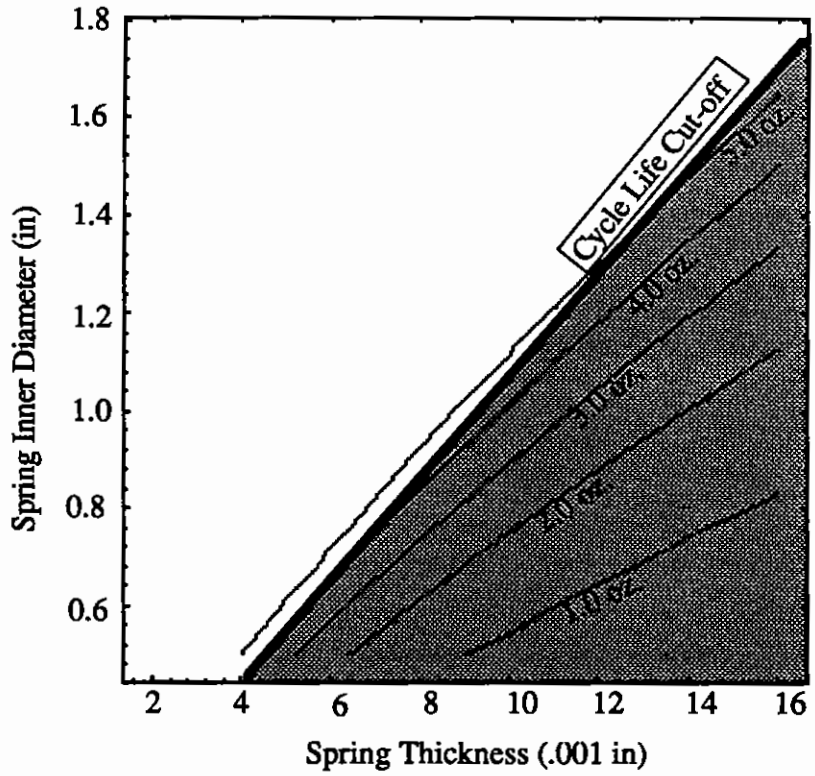

Figure 4.4.3. Weight of Springs (in oz) to meet 40 lb. Force Requirement

From Figures 4.4.2 and 4.4.3, we can see that there is no single spring which will satisfy all of our requirements, therefore, I did not use them in the hand/wrist design. This does not indicate, however, that there are no applications for which bias springs could be useful. For low travel, low torque, high speed servo control, constant force springs would work well. In addition, applications where a large, constant baseline force or torque is needed with small controlled variations about that force or torque, a small motor and constant force spring combination would have a huge advantage over a larger motor alone.

4.5 Making the Optimum Motor Choice

In an ideal world, one could develop a complete (and enormous) equation which, when the design constraints were entered, could be optimized to produce specifications for the best motor for the task at hand [Anderson, 90]. For most applications, however, we need to make do with 'off-the-shelf' motors. Since this is such a common decision that needs to be made for most mechanical designs, I have attempted to compile a series of steps to aid in motor selection of permanent magnet and series wound DC motors.

The most common method engineers employ when choosing motors is estimating the power required for a task, examining the specification sheets for several possible motors in that set, and then deciding on a case by case basis which will perform as desired and which are unsuitable. This is an inefficient method which is time consuming, non-repeatable, and can lead to choosing a motor that is not very well suited for an application. As an alternative, my proposed method is similar to the series of design space filters proposed in [Ward, 89] except that I am dealing with only one component - motors. In this method, a pool of possible actuators is generated and a series of simple restrictions are applied to quickly narrow the choice to the handful of motors that will perform as needed. This method involves compiling a database of known motors which can be used again later for other design tasks.

There is no complete set of simple filters that will work for every application, since the most important requirements in every application vary greatly. However, the performance filters presented here are sufficiently general and adaptable that they will most likely narrow the motor pool by 80-90% for a wide range of mechanical design problems. To further narrow the choice, I have included guidelines for development of additional task-specific filters.

This approach, while it may seem simple in concept and application, employs performance filters which are not necessarily intuitive. Because of this, I will spend some time to develop the form of the filters.

4.5.1 Determining Your Motor Requirements

Before looking for motors to complete a task, the specific requirements of that task should be known. Where exact numbers are not possible (such as mass of the payload which can be variable), an expected range should be specified. The relative importance of the system requirements (as dictated by your application) will determine in what order the specifications will be used to pare down the motor set.

The requirements for each motor in the hand/wrist actuator package specified by the design constraints outlined in section 3.0, are summarized in Table 4.5.1.

Parameter	Value
Size (radius)	smaller than 51 mm [2"]
Size (length)	smaller than 360 mm [14"]
Mass	less than .34 Kg [.75 lbm]
Peak force	180N [40 lbs]
Max. continuous force	90N [20 lbs]
Acceleration	27 m/s^2 [1067 in/sec^2]
Hand inertia to be driven	Nm? [.056 $in\text{-}oz\text{-}s^2$]
Estimated power range	20-60 Watts

Table 4.5.1. Physical Constraints on the Motors

The power range is a good specification to initially define the motor pool. It is prominently featured on motor specification sheets and in catalogs, and will include the complete set of all motors that can meet the requirements while being smaller than the set defined by size or weight parameters. I chose a larger range than I had specified for the performance since many motor manufacturers will quote *consumed power* rather than maximum continuous *shaft power* (the figure we're actually interested in). Some motor manufacturers will actually go so far as to quote maximum consumed power at stall (10

seconds before the lacquer on the windings burns off and shorts the motor out) - examine the motor specification sheets carefully.

4.5.2 Prefiltering with Size and Weight

The motor pool can be further restricted by "prefiltering" with the dimensional requirements for the motor. In many machine design applications - especially robotic applications, physical size or shape will often remove a large number of motors from the pool defined by power. This is a simple, "yes or no" filter to run on the motor pool.

For the hand/wrist application all motors heavier than .75 lbm. [.34 Kg] or having diameters larger than 2" [51mm] were discarded.

4.5.3 Performance filters

The first set of filters are designed to determine the subset of the motor pool that can perform the specified task. For a motor to complete the required task, it must pass both of these filters.

Acceleration

For most servo applications, speed and acceleration are desirable attributes, whether they are minimum no-load accelerations or a minimum speeds and accelerations with a standard payload. Keeping the required task in mind, find minimum acceleration profile (as in section 3.3) and use it to apply the acceleration filter.

For the hand/wrist, since the motor must be able to move a cable (attached to the hand) 6 inches in 150ms, we can discard all the motors from the pool incapable of producing the minimum acceleration profile from Section 3.3 (corresponding to 1067 in/sec^2 [27.35 m/sec^2]). To determine a motor's maximum acceleration capability under the load of the hand, we can use the impedance matched gearing which gives us the optimum gearing for acceleration [Pasch, 83]:

$$r' = \sqrt{\frac{J}{M}}\ in^* \qquad (4.5.1)$$

where J is inertia of the motor and transmission and M is the mass of the load.

Since we are translating rotary motion into linear motion, the gear ratio (equal to the inverse of the transmission ratio) has units of length equivalent to the radius of a pulley required to produce that gearing. Using the optimum gearing for a given motor will give us a maximum acceleration of :

$$a_{max} = \frac{T_{max}}{\sqrt{J}} \times \frac{1}{2\sqrt{M}}\ (in/sec^2) \qquad (4.5.2)$$

where T_{max} is the maximum motor torque (at stall).

For very short motions, (equation 4.5.2) may be used to compare acceleration values between motors. For longer accelerations, however, the back EMF of the motor will cause the torque to drop off as the motor speeds up (unless the current can be kept constant). This becomes more important if the maximum velocity reached in an acceleration profile is a significant percentage of the motor's peak velocity. If we assume that the torque/speed curve for the motor is linear, then we can find another performance filter that is a function of the torque/speed slope (T_{max}/ω_{max}), the inertia of the rotor and the transmission, the mass of the load, the distance to be traveled, and the time requirement.

Assuming that we will continue to use the optimum gear ratio, r', for acceleration, the acceleration available is similar to equation (4.5.2) except that we substitute $T(\omega)$

$$T(\omega) = T_{max} - \omega\left(\frac{T_{max}}{\omega_{max}}\right) \qquad (4.5.3)$$

---

* This is similar in form to power rate (T_{motor}^2/J_{motor} (Kw/s)) - a measure of *deliverable* torque from an actuator during acceleration advocated by [Arnold, 85] as a "figure of merit" for motors.

for T_{max}, and then substitute for ω,with $\omega(a, t)$

$$\omega = \int_0^t a\, dt\,. \qquad (4.5.4)$$

For clarity I introduce and substitute two constants C_1 and C_2 here equal to:

$$C_1 = \frac{1}{2\sqrt{JM}} \qquad C_2 = \frac{T_{max}}{\omega_{max}}\,. \qquad (4.5.5)$$

The equation 4.5.2 for $a_{max}(t)$ now becomes:

$$a_{max}(t) = C_1(T_{max} - C_2 \int_0^t a_{max}(t)\, dt). \qquad (4.5.6)$$

The initial conditions (@t=0) for the acceleration from rest are: d=0, ω=0, and a_{max}=C_1T_{max}, which leads us to a solution of:

$$a_{max}(t) = C_1T_{max}(e^{-C_2t}) \qquad (4.5.7)$$

This acceleration expression will give us acceleration profiles which deviate from the straight-line profiles of Figure 3.3.2 with an exponential decay as the motor velocity approaches the no-load motor velocity (see Figure 4.5.1).

To produce the performance filter, we need to integrate equation (4.5.7) twice with our initial conditions to find an expression for the distance traveled:

$$d = \left(\frac{T_{max}C_1}{C_2^2}\right)e^{-C_2t} - \frac{C_1T_{max}}{C_2^2} + \frac{C_1T_{max}}{C_2}t$$

$$d = \left(\frac{T_{max}C_1}{C_2^2}\right)[e^{-C_2t} - 1 + C_2t] \qquad (4.5.8)$$

substituting for C_1 and C_2 we get:

$$d = \left(\frac{\omega_{max}^2}{2\sqrt{JMT_{max}}}\right)\left[e^{-\left(\frac{T_{max}}{\omega_{max}}\right)t} - 1 + \left(\frac{T_{max}}{\omega_{max}}\right)t\right] \qquad (4.5.9)$$

This messy-looking expression is the acceleration performance filter: if half the allotted time (t) is substituted in, and the resultant distance (d) is less than half the required distance for the allotted time, then the motor will not be able to perform the required acceleration profile.

We can now remove all the motors from the set which cannot meet this acceleration requirement.

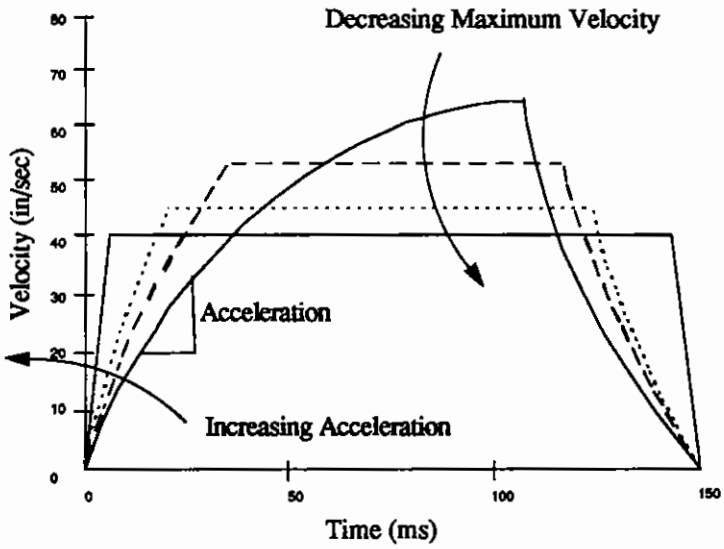

Figure 4.5.1. Acceleration Profiles with Velocity Dependant Accelerations.

Torque

At the strength end of its performance range the motor needs to be able to pull on a cable with 180N [40 lbs]. Even though any motor with enough gearing down is capable of producing 180N at stall, if that gear ratio r_g is lower than the optimum acceleration ratio r' (i.e. the transmission ratio is higher), there will be no single transmission that will allow the motor to meet all of the performance specifications.* Therefore, all the motors with a required r_g lower than r' were discarded.

Additional Filters

After the performance filtering, only two motors remained from the 30+ which had been considered. Since the number was small enough to be manageable, the last decision was made taking all the rest of the requirements into consideration. If, however, my performance requirements for the motors were low enough that a large group of motors were available, I would have the opportunity to apply additional filters such as:

Weight: One can always decide to use the lightest motor left.

Transmission ratio: If one needs a backdriveable system, a lower transmission ratio will usually be better.

Power consumption: Use the motor Constant K_m, a commonly specified indication of how effectively the motor converts electrical energy into torque (equal to the ratio of Peak torque at stall to $\sqrt{\text{watts}}$ dissipated at 25°C).

Maximum operating temperature: many magnetic materials (such as Fe-Ni-B) suffer decreases in magnetic field strength at elevated temperatures, and will need cooling if they are to be run hard. If you have a hard-to-cool application, you probably want to pass over these motors.

---

* It should be noted that this is not *entirely* true since a motor with an a_{max} much larger than a_{req} may be able to satisfy the torque and accelerations at an r_g somewhat lower than r'. However, since dissipative losses inside the motor increase quadratically as the ratio of r_g/r' deviates from 1 [Pasch and Seering, 83], the motor must supply more power to perform the same task, and will tend to be heavier.

The Maxon RE 20 38

For the hand/wrist actuator package, the order of importance for meeting the specifications was chosen to be 1. Weight 2. Backdrivability 3. Size.

I chose the Maxon RE 20 38 motor because it satisfied all of the performance requirements, and had an available low-backlash planetary gearbox in the ratio 4.33 which was extremely close to the optimum ratio (4.31) for a .25" shaft . The planetary gearhead meant an additional speed reduction did not have to be added to what was already going to be a crowded gearbox. Also, I felt that the 1" diameter offered greater design flexibility inside the 2" maximum actuator package thickness.

4.5.4 Problems

One of the biggest problems with this filter method is it is possible to filter away the entire pool of motors. Also, the process is not impervious to human misjudgment, so if the performance specifications are wrong, or later filters are applied in an inappropriate order (least important first), then the 'best' motor may be lost in the process. However, if the filtering process is done on a spreadsheet like Excel$_{tm}$ or Lotus 123$_{tm}$, the performance constraints can easily be changed or relaxed until enough motors pass through that the remaining guidelines can be applied.

4.6 Cable Materials

One of the limiting factors in cable-driven robots is the cables themselves. While they have the advantage of allowing us to place the power source far from the actuated member without much increase in mass, we have seen that there is a corresponding drop in stiffness and control bandwidth. Cables also tend to be fragile, and will not suffer mistreatment gladly (a pampered cable is a happy cable). To varying degrees, all cables will self-abrade when wrapped onto capstans, self-abrade when run around small diameter pulleys, pull fibres from adjacent cables, stretch, creep, fatigue, exhibit non-linear spring constants, slip off pulleys when not under tension, snarl, kink, and fray. But despite this long list of shortcomings, a better substitute has yet to be found.

There are many cable materials ranging from steel to the newer polymer "super-fibres" *, each with their own advantages and disadvantages. For robotic applications on the scale of the WAM wrist/hand several types were considered. The cable materials considered for the design are introduced briefly here and then compared in Section 4.6.3.

4.6.1 Steel

Steel is a widely studied cable material and up until now, steel cables have been the most common cable material used for load bearing and actuation (including airplane control surfaces, bicycle brake cables and as tension members in suspension bridges). They are reasonably stiff (a K of 970 lbs/in for 10" of 170 lb. test cable (from Sava Industries)) and will not mutually abrade as much as many of the polymer cables. Steel 150 and 250 lb. test cables make up most of the cabling in the WAM and have served well over many hours of use. The biggest problem with steel cables is their rapid fatigue and breakage when run

* A "super-fibre" is defined as having a modulus greater than 55 GPa and a tenacity greater than 2.5 GPa [Hongu and Phillips, 90]

over small pulleys. With a safety factor of 1.0, these cables require a pulley diameter to cable diameter ratio (D/d) of 15 to 50 or more (depending on fibre size in the cable). Even for a steel 7x49 wrap, 170 lb tst . cable, this means a pulley .8" or greater (limiting the design possibilities greatly). In the interest of a light, compact design, an alternative was sought.

4.6.2 The new "super-fibre" cables

The man-made polymer super-fibre cables can be spun into very small fibres with high yield strength and high modulus. Some of these materials also have high notch strength, and can be made into cables which can be wrapped around small pulleys. This makes them much more suitable for compact designs. With these characteristics, however, come a host of other problems that make it very important to match the cable material carefully with the application.

Kevlar

Kevlar™, an aramid fibre made by the DuPont Chemical company, is one of the best known polymer super-fibres. It is used in applications such as bullet-proof vests, fire-fighting clothing, and mooring ropes where toughness and heat resistance is required. As a cable material, however, its high self-abrasiveness makes the life of the cables very short . (See Figure 4.6.5)

Spectra

Spectra™ is an Ultra-High Molecular Weight Polyethelene (UHMWPE) made by Allied Fibre. Its low specific gravity make it useful for light-weight composites for protective equipment such as helmets, and Spectra 1000 is available in small braids for use as high performance kite string. It is very strong, and very stiff, and has very low self-abrasion, high fatigue strength, but its use has been limited in cable and rope applications because of its extremely high creep. (see Figure 4.6.2)

Vectran

Vectran™ is a polyester-polyarylate fibre more recently developed by Hoercht Celanese. It's main features are nearly zero creep and high shock absorbancy while still exhibiting the strength characteristics of a super-fibre. Some preliminary testing work done at Woods Hole Oceanographic Institute indicate some braids of Vectran have non linear spring constants and slightly bulkier cables than Spectra or Kevlar, but these tests were done on heavy braids which may have more constructional stretch* than the small braids required for applications of the scale of the WAM. While testing cables for the robot, Vectran was unavailable in small braids, but its interesting properties may make it useful for robots where cable creep cannot be tolerated (see Section 8.0 Future Work).

Other Fibres

There are other similar fibres commercially available in Japan including Ekonol™ and Technora™ [Hongu and Phillips, 90]. Ekonol is a liquid crystal aromatic polymer from Sumitomo Chemical Company that is similar in form to Vectran. Technora is an aramid fibre produced by Tejin Company that is similar to Kevlar but produced by a different process. They are currently in use in many composite products, but were not readily available for testing.

* Constructional stretch consists of the individual fibres of the cable settling together to make a more compact braid. Once all the fibres in the cable have seated properly, elastic stretch of the individual fibres dominates the spring constant of the cable.

4.6.3 Comparisons

Stiffness , Strength, and Density

As we saw in Section 2.1.1, stiff transmissions are desirable. To this end, we would like to have cable materials with a high Modulus (ratio of stress to strain). In addition, a high strength material can be made into a slender cable, allowing us to run it on a small pulley. Finally, the density of a material will determine how heavy a particular cable will be. The density, Tenacity (Tensile Strength) and Modulus (Elastic Modulus) of each of the materials under consideration is listed in Table 4.6.1 [Galasso, 89], [Beers, 90], [Hongu and Phillips, 90], and [Oberg et al, 85]:

Fibre	Density g/cm^3	Tenacity GPa	Modulus GPa
Spectra	0.95	3.72	200
Kevlar 29	1.44	2.79	66.7
Kevlar 49	1.45	2.94	102
Technora	1.39	3.06	70
Vectran	1.40	2.84	80
Ekonol	1.40	3.80	133
Stainless Steel	7.80	0.69	207

Table 4.6.1 Density, Tenacity and Modulus Data for Several Cable Materials

From the data in Table 4.6.1, we can see that if we were to make up cables of Spectra and steel that had the same stiffness, the Spectra cable would be about five times as strong, and have one eighth the mass. Vectran cable of the same stiffness would be ten times as strong as the steel, but have only half the mass.

Creep

Creep, as distinct from stretch, is a slow permanent change in dimensions from long exposure to stress or high temperature. The molecular structure of some of the super-

fibres make them susceptible to creep which leads to a relaxation of pretension in cables, and can introduce backlash into a cable drive unless the tension can be actively maintained.

The data presented here for creep are from experiments conducted at MIT on 150 lb. test Spectra 1000 cable (see Figure 4.6.1), and experiments on 12.7 mm Spectra 900, Vectran HS and Kevlar 29 ropes conducted by the Whitehall Manufacturing Corporation and reprinted from [Beers, 90] (see Figure 4.6.2).

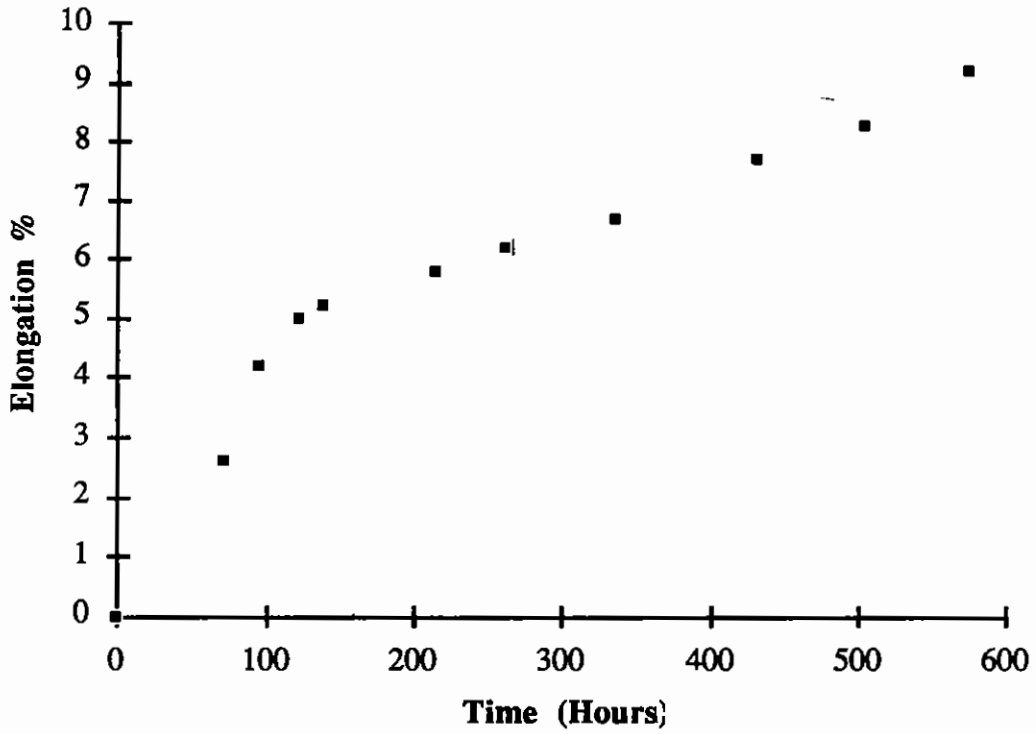

Figure 4.6.1. Elongation of 150 lb.Test Spectra 900 Cable Loaded to 45 lbs vs.Time

The difference between the initial creep rate and that at 100+ hours may be from constructional stretch and fibre alignment during the initial loading period.

The 12.7mm rope in the Whitehall experiments is considerably larger than the 1 to 2mm cables that would be appropriate for small robotic use, but it is presented as a useful comparison between the materials, and not as an indication of how cables of the size we are

interested in would perform. The Vectran exhibited no creep for the duration of the test while the Spectra exhibited very pronounced stress relaxation.

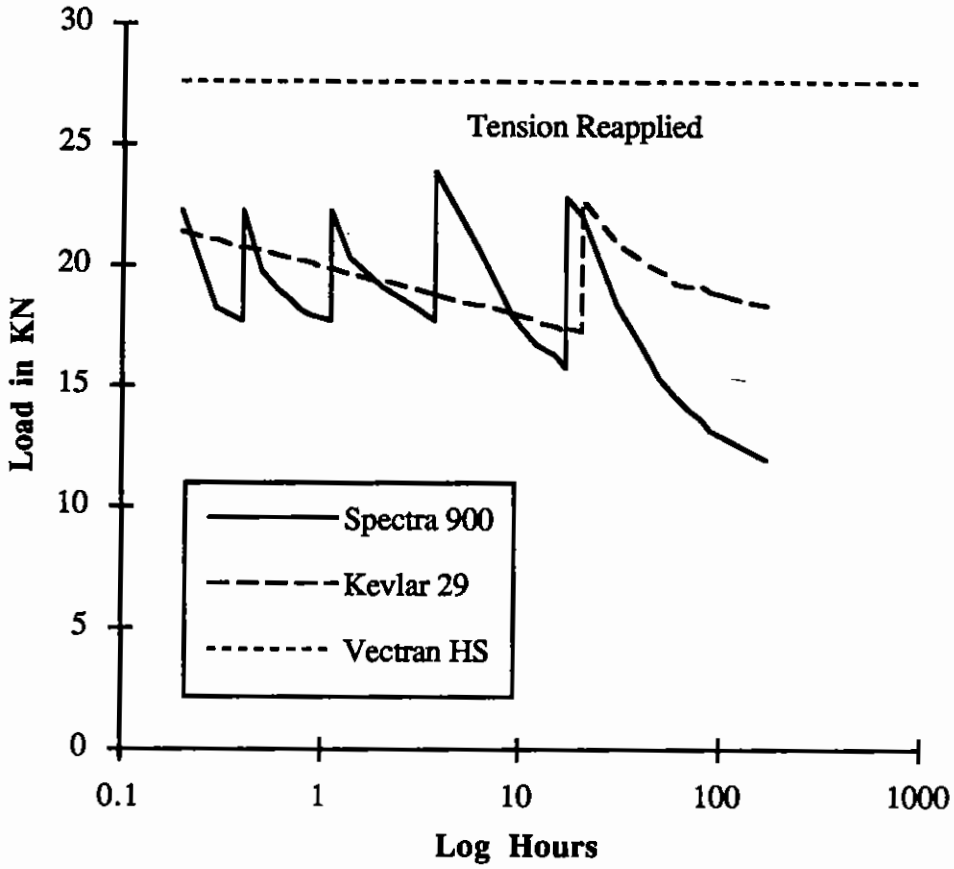

Figure 4.6.2. Stress Relaxation in Spectra 900, Kevlar 29, and Vectran HS, 12.7mm Rope Loaded to 17% of the Breaking Strength and Retensioned upon Relaxation. Whitehill Manufacturing Corporation.

Fatigue

Fatigue is the tendency of a material to break under repeated stress. To evaluate the fatigue life of the 150 lb. Spectra Cables under the type of loading we could expect inside the actuator package, I loaded a cable with a weight, and cycled the cable onto and off of a capstan in the apparatus shown in Figure 4.6.3.

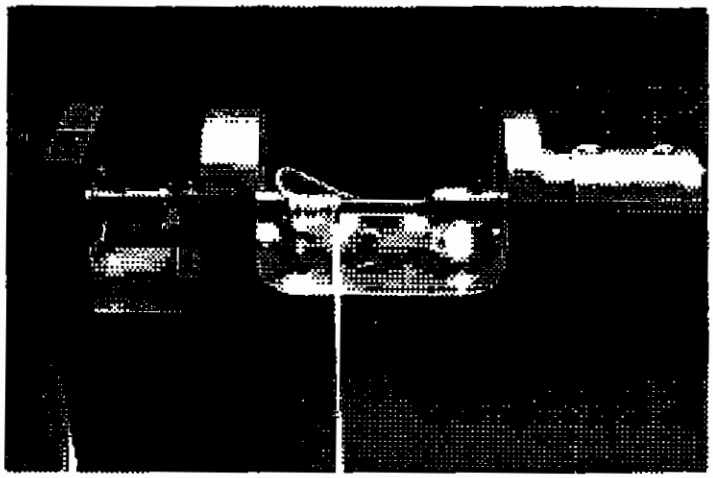

Figure 4.6.3 Cable Fatigue Testing Apparatus.

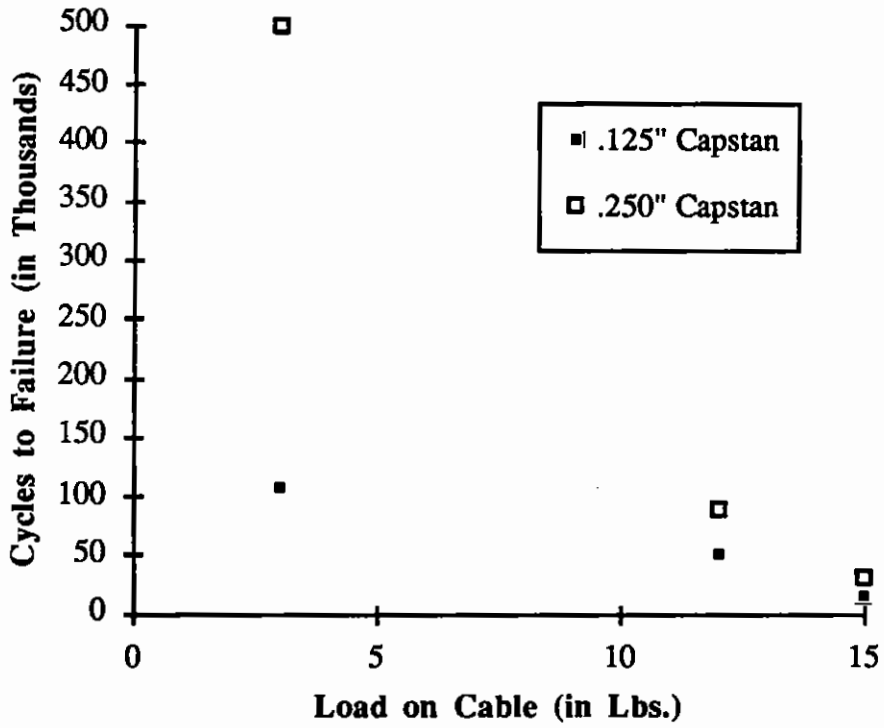

Figure 4.6.4. Self-Abrasion Life of 150 lb. Test Spectra 900 Cable. Wrapping onto and off of a Steel Capstan.

The results are shown in Figure 4.6.4. The cause of failure for the cables seemed to be "picking" (cables pulling fibres from adjacent cables). This "picking" failure is a somewhat liberal definition of fatigue failure since the fibres themselves were not fatiguing, but this form of stress and failure will be found in a capstan drive system, so it was deemed more relevant than the more traditional "whipping" or axial loading fatigue experiments. The capstan diameter to cable diameter (D/d) for this experiment was 3 for the .125" capstan, and 6 for the .250" capstan.

The data comparing the fatigue life of Spectra, Vectran and Kevlar is from experiments that were conducted by Whitehall Manufacturing Corporation and presented in [Beers, 90]. All tests were bend-over-sheave fatigue life of 12.7mm rope on 9.55" diameter pulleys (a D/d of 19)(see Figure 4.6.5), and showed cycle lives that correlated with the small cable tests.

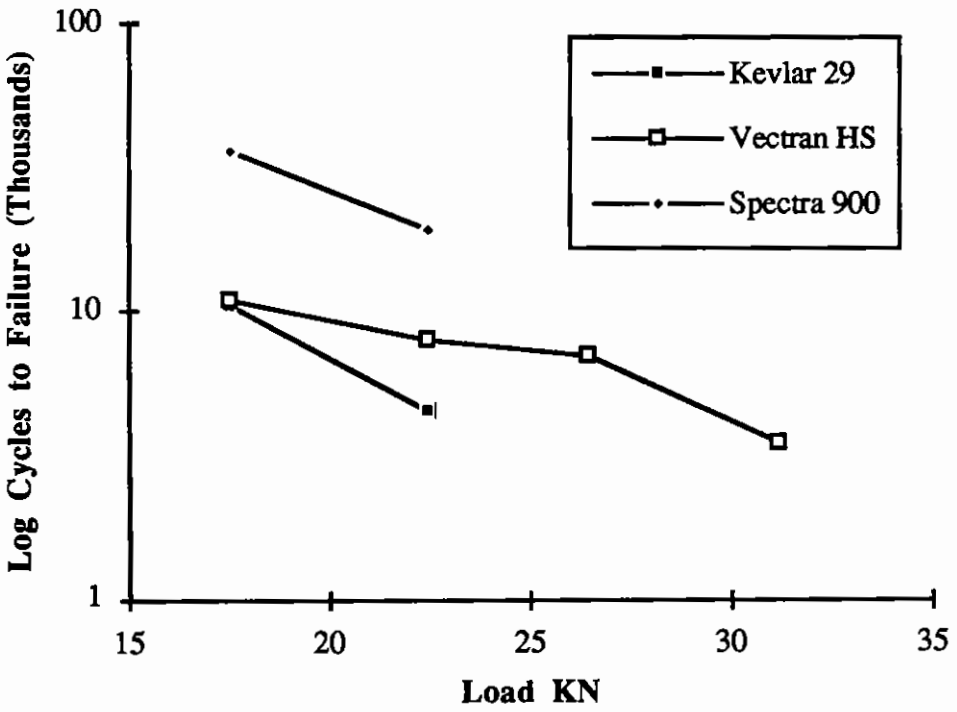

Figure 4.6.5. Bend-Over-Sheave Test on Spectra 900, Kevlar 29, and Vectran HS 12.7mm rope on 9.55" diameter pulleys. Whitehill Manufacturing Corporation.

Because of its availability, and low self-abrasion Spectra cable was chosen for the first application. The high creep characteristics were not considered to be a problem with the *n+1* design. The 2*n* axis of the wrist was to be initially cabled with Spectra, and when Vectran became available in small braids, that axis would be recabled with Vectran to compare the durability of the two materials in this robot.

5.0 The Design of the Actuator Package

This section details the design and construction of the actuator package including motors and cable routing. Mechanical drawings for actuator package mounting plates and the pulley mounts are included in Appendix B.

5.1 Motor modifications

The Maxon motor planetary gearheads came with a .197 in [5mm] dia shaft, which was capable of taking a 3.6 lbs [16N] maximum load at the tip. This was far less than the 40 lbs [180N] necessary for the tendon actuation. Therefore the gearbox had to be modified so that it could take the loading required of it. Since the loads were to be so high, it was necessary to support the .25" shaft from both ends to avoid bending. This required either removing one of the two shaft support bearings from the end of the gearbox, or connecting the motor to the capstan through a flexible coupling. In the interest of saving weight, I modified the gearbox rather than adding additional parts.

Since the endcap of the gearbox no longer had to house two bearings, it could be made smaller, and most importantly, lighter. Also I could replace the gearbox bearings with FAG high precision, low profile R1624 bearings which could take the required load. A new shaft could also be made for the motor and pressed into the retainer for the planet gears, and this could be hollow (see Figure 5.1.1).

The outer shell of the ring gear was also much thicker than it needed to be (considering the planet gears are plastic, and the gearbox was not expected to take any

lateral loading in the current design, ring gear was overdesigned), so .050" [1.27mm] was removed from each motor's gearbox diameter. The weight savings from these modifications is 1.1 oz [31 g] for each motor. (.8 oz [22 g] from the endcap modification, .3 oz [9g] from the ring gear modification). For the entire motor package this reduces the weight by 6.6 oz. [186 g], a significant saving.

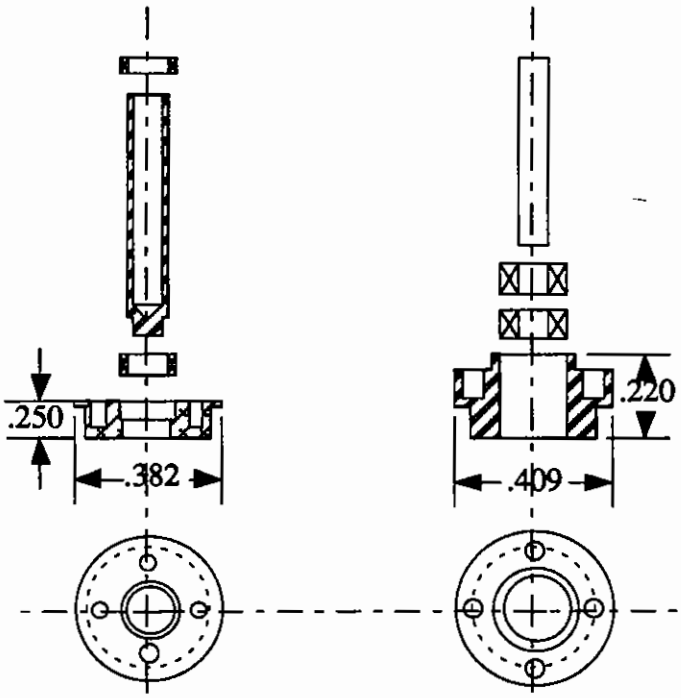

Figure 5.1.1. Crossections of the New and Old Endcaps

5.2 Actuator Package Layout and Construction

The Maxon motors have an optional incremental encoder which has a compact profile. Unfortunately, it wasn't quite compact enough, and the encoder enclosure overhung the motor body by .26" [6.6mm]. This meant that the motors had to be staggered in order to close-pack (see Figure 5.1.2).

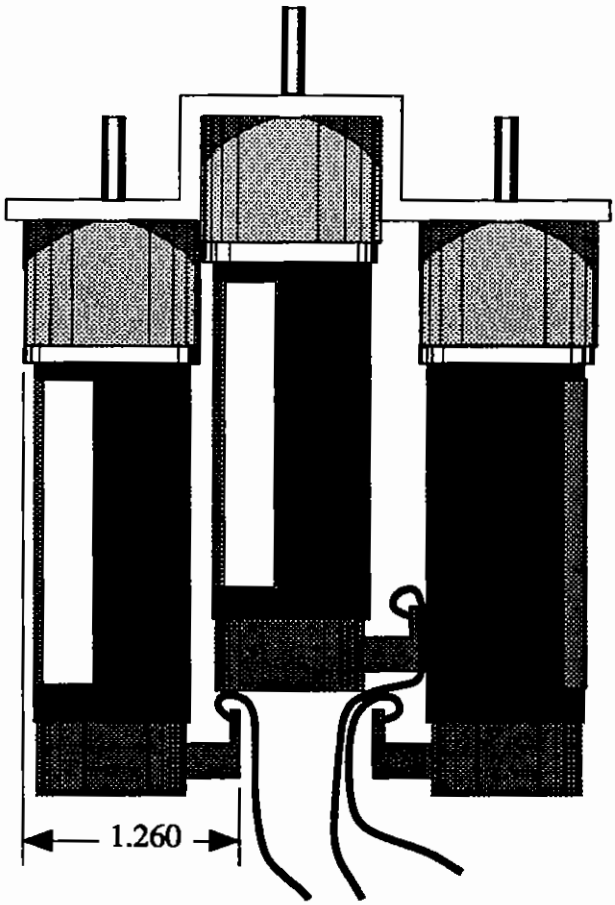

Figure 5.1.2. Closest Packing for Motors with Encoders

5.2.1 Pulley mounts

If we were going to use a "bundle" configuration with the axes of the motors aligned with the direction of the cable, we needed either to run the capstan at right angles to the motor shaft, or have the cable turn a corner. The "cable turning the corner" design was selected because it eliminates additional power transmission elements from the design (and any additional backlash, friction, and mass they might incur), and lets us simply use an idler pulley to turn the cable direction. This pulley will also let us measure tendon torque fairly accurately by mounting strain gauges directly onto the pulley support arms (see Figure 5.1.3).

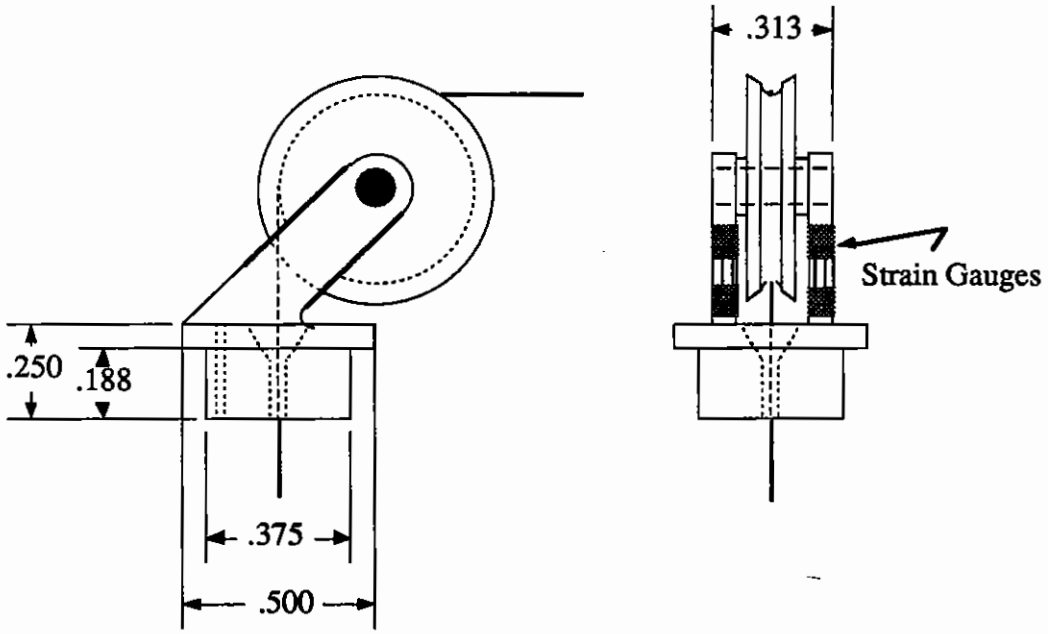

Figure 5.1.3. Pulley Mounts with Strain Gauge Attachments.

5.2.2 Cable layout

Since the motors we chose had a 1" OD, the smallest bundle that still met the 2" forearm requirement was the simple six (shown in Figure 4.3.2). Now, the next step was to bring the seven cables down from the wrist in an orientation that would not cause them to slip off the hand pulleys, and to run them out to the capstans which were going to reel them in. Since we are wrapping cables onto a capstan, the more wraps the capstan has collected, the greater the angle (Θ) between the straight line distance between the pulley output and the capstan uptake (Figure 5.1.4). It is highly desirable to maximize the distance between the pulley and the capstan because at some critical angle Θ, the cable will jump from neatly wrapping down next to its neighbor to wrapping over itself. Cables then pull through the cable layer below, get jammed and start ripping each other apart, and the capstan diameter effectively changes.

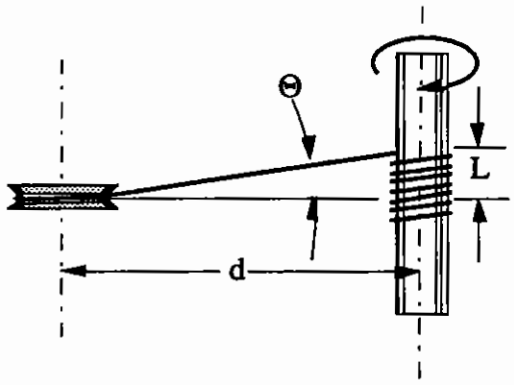

Figure 5.1.4. Wrap Angle (Θ),Center Distance (d), and wrap length (L) for a Cable Wrapping onto a Capstan

With all this in mind, the 'optimum' cable layout needed to be found for this application. In preliminary testing, we found that the wrist is less likely to drop cables if they enter the wrist pulleys from near the outside of the forearm tube. DesignView™, a variational geometry program, was employed to determine the 2-D layout of cables and pulleys that would maximize the average distance from pulleys to the capstans they fed while placing the cable exits as close to the tube wall as possible (see Figure 5.1.5). This meant several pulley/capstan pairs would be a little close (small d's), but that was considered acceptable since several of the cables would not have to travel the full six inches specified in the design, and therefore they would not require the same wrap length L. See Figure 5.1.6 for an exploded view of the actuator package.

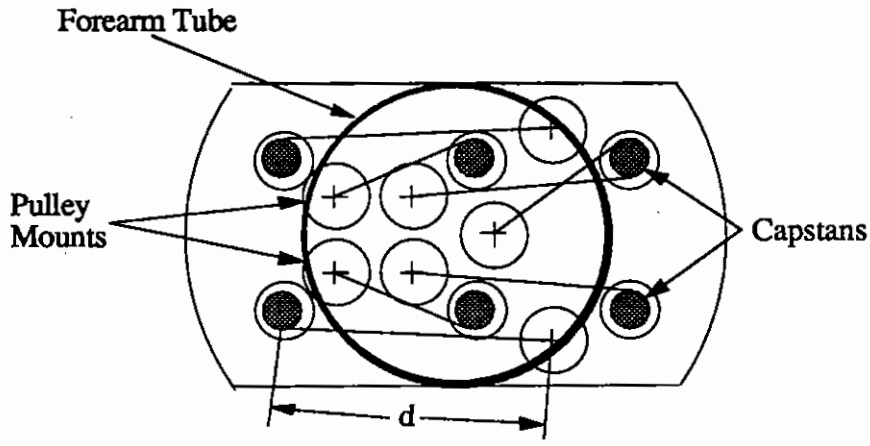

Figure 5.1.5. Top Plate of Actuator Package with Cable Distances Maximized.

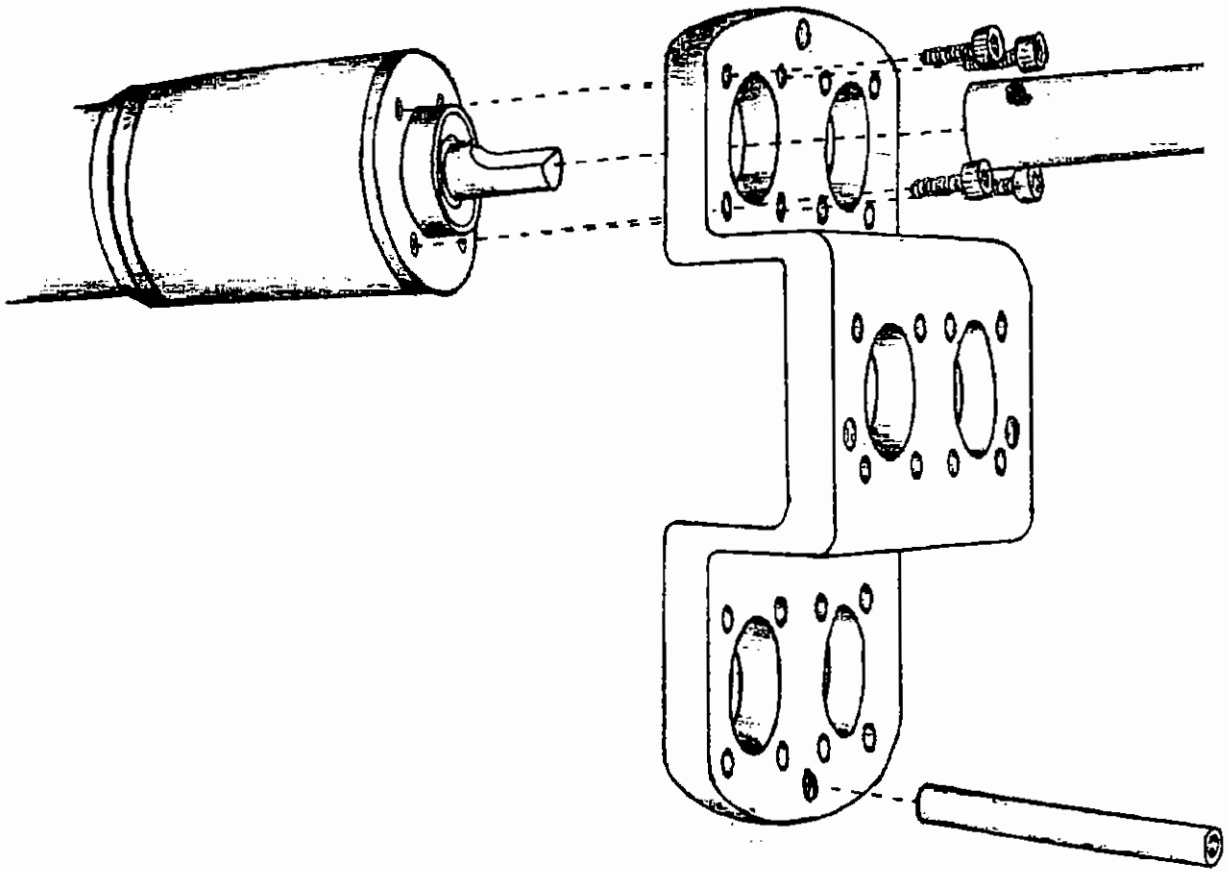

Figure 5.1.6 Exploded View of the Actuator Package.

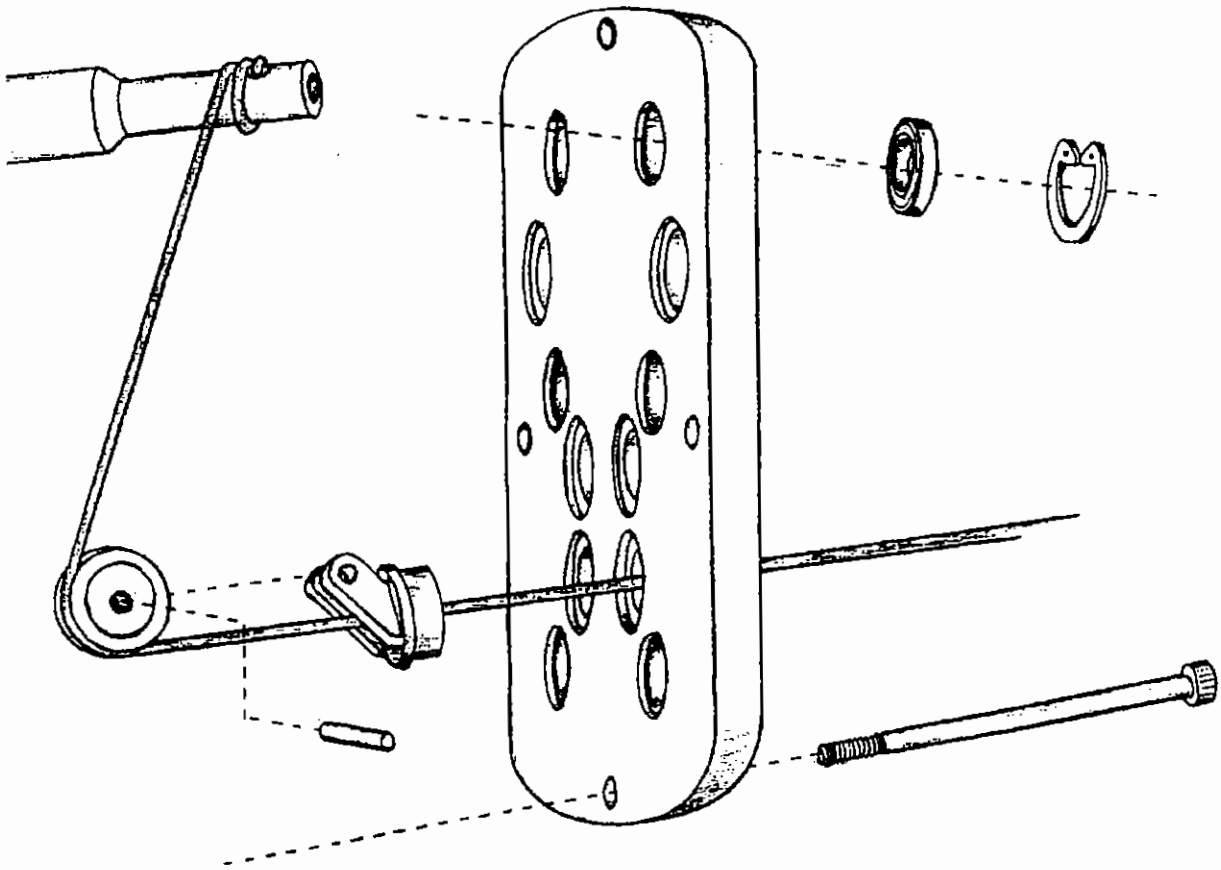

The final assembly of the gearbox was done without the strain gauges for the tendon tension sensing hooked up (see Figure 5.1.7). This was so the early experiments with the hand control could be done without worrying about damaging the strain gauges, and design errors could be found and corrected without the time investment of the micro-soldering required for the pulley mounts.

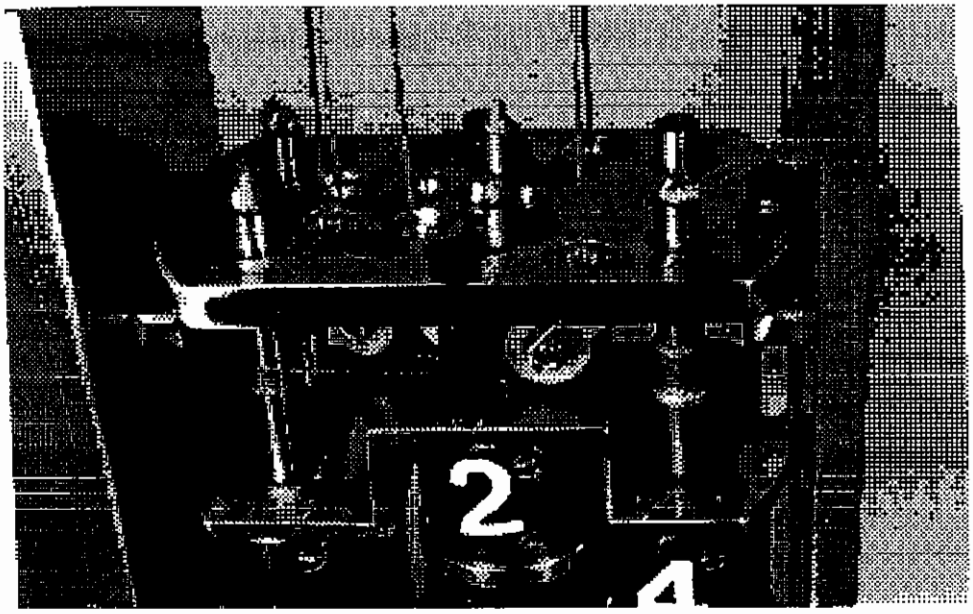

Figure 5.1.7 The Assembled Actuator Package During Preliminary Testing.

6.0 Implementation of the Tendon Tension Control Loop

As we saw in Section 2.1.2, having tendon tension feedback is desirable for force control since small local variations in the tension can be measured by the strain gauges mounted on the pulley base and fed back to the controller for smoother force output.

Torque loop experiments were conducted independently of the actuator package testing. These included attaching strain gauges on one of the pulley mounts (see Figure 6.0.1) and running a linear spring loaded cable over the pulley to the capstan, using the same motor apparatus that had been used for the cable fatigue tests (see Figure 6.0.2).

Figure 6.0.1. Pulley Mount with Strain Gauges

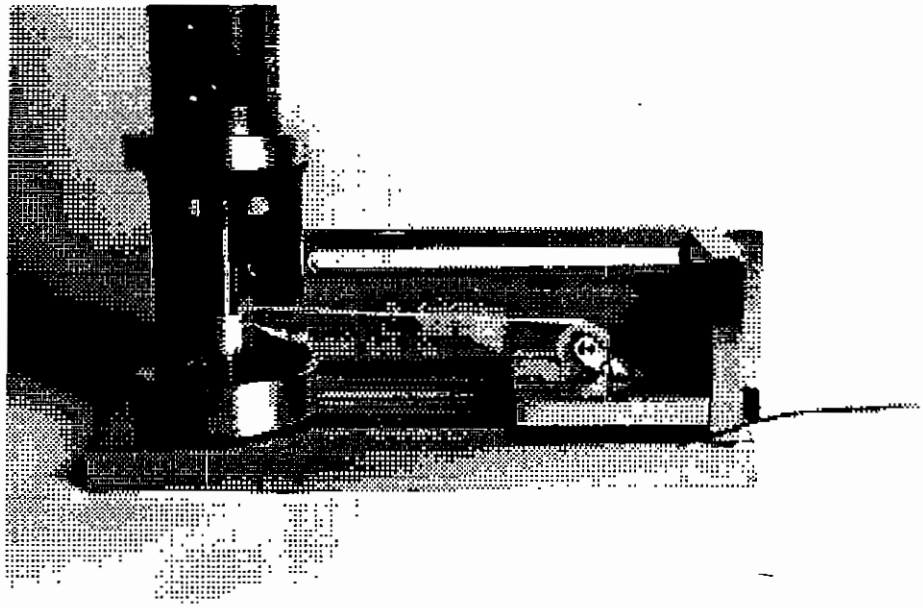

Figure 6.0.2. Tendon Tension Testing Setup

For the open loop testing, the motor was sent a triangular force (current) trajectory without any force or position feedback. The current commands were sent using a Motion Engineering Motion Control board which delivered the current changes in fairly coarse steps. (The output force resolution was in .35 lb [1.6N] increments corresponding to a 1 bit change.) The force trajectory followed by the un-compensated motor was measured by the strain gauges on the pulley mount, amplified using an Artificial Creatures, Inc. eight channel in-line Amplifier board, and sampled at about 1 KHz using a C10-AD16 A to D board made by Computer Boards, Inc. A comparison of the open-loop force trajectory to the commanded force trajectory is shown in Figure 6.0.3.

For the closed-loop trajectories, the strain gauge measurements were used both to record the actual force from the motor, and to determine the deviation from the commanded force (see figure 6.0.4). The same commanded force trajectory was re-run with the torque feedback and the resultant closed loop trajectory is shown in Figure 6.0.5.

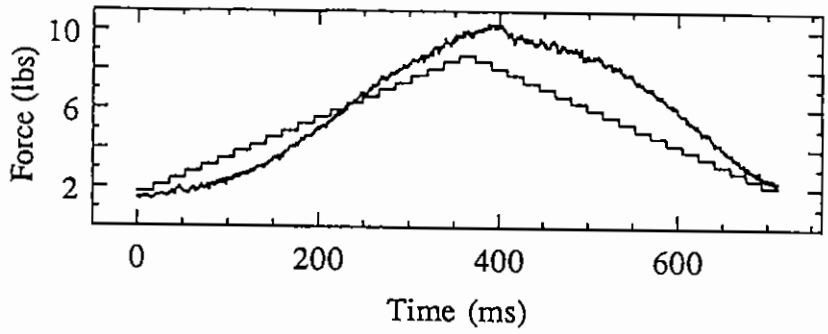

Figure 6.0.3. Open Loop Force Trajectory.

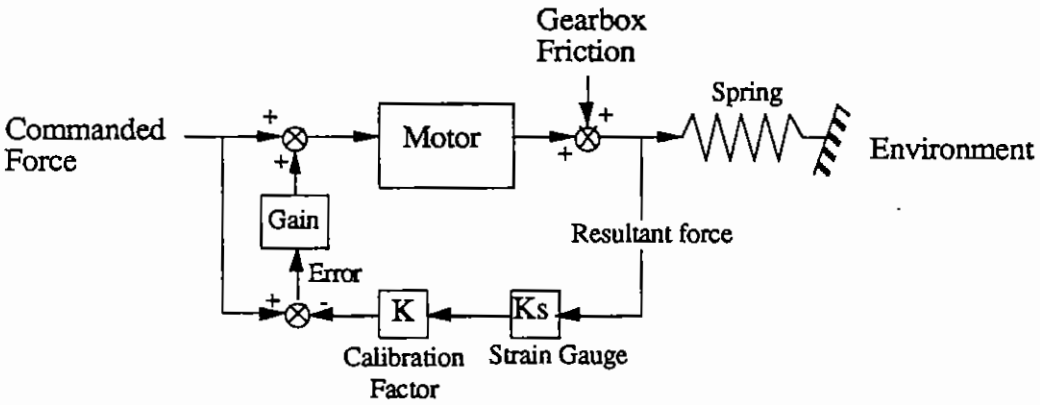

Figure 6.0.4. Force Feedback for Closing the Torque Loop.

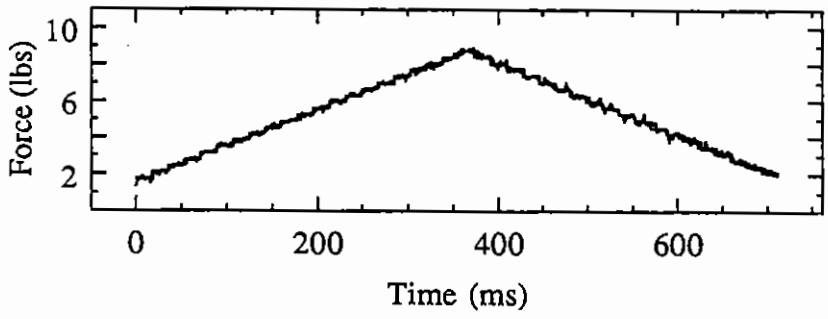

Figure 6.0.5. Force Trajectory with a Force Feedback Gain of 60.

Figure 6.0.6 shows a comparison between the errors measured for both trajectories. With the feedback loop, some of the effects of the gearbox friction, and unmodeled spring and motor dynamics on the force trajectory were reduced, and the trajectory was very closely followed.

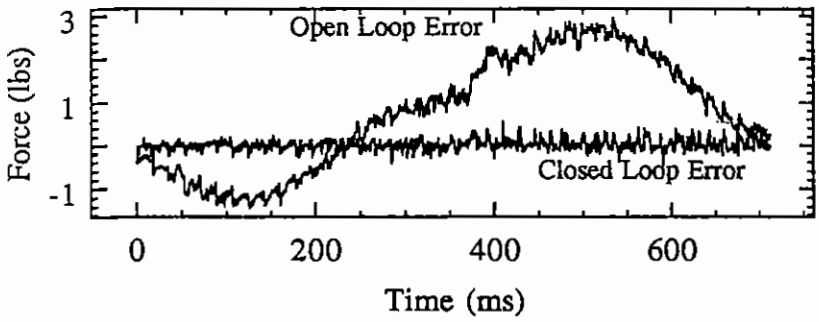

Figure 6.0.5. Error Comparison Between Open Loop Trajectory and Force Feedback with a Gain of 60.

7.0 Results

The actuator package and a prototype of the wrist/hand were built and mounted inside a forearm "mockup" (See Figure 7.0.1) to test the performance of the wrist/hand/actuator package system before attaching them to the WAM. The hand was successfully run under force and position control and exhibited smooth backdriveability, quick response, and resistance to abuse. The passive curling of the fingers allowed the hand to conform to most objects (see Figure 7.0.2). The speed of the hand is excellent, and the motors are even stronger than required (strong enough, we found, to pull the hand apart if the control code crashes).

It remains to be seen what effect the new forearm will have on the dynamics and catching ability of the WAM. The wrist/hand and actuator package, however, are robust and the motors seem to be well matched to the hand.

The Spectra cables have been far exceeding expectations. They are stiff, tough, and wrap neatly onto the capstans even at fairly extreme angles. It was found that when the cables were allowed to go slack and the cables moved around before they were retensioned, one of the cables would occasionally fail to re-seat in the pulley groove. Under simple position control, this did not affect the function of the actuator package greatly since the controller was not bothered by the additional friction caused by the cable riding on the

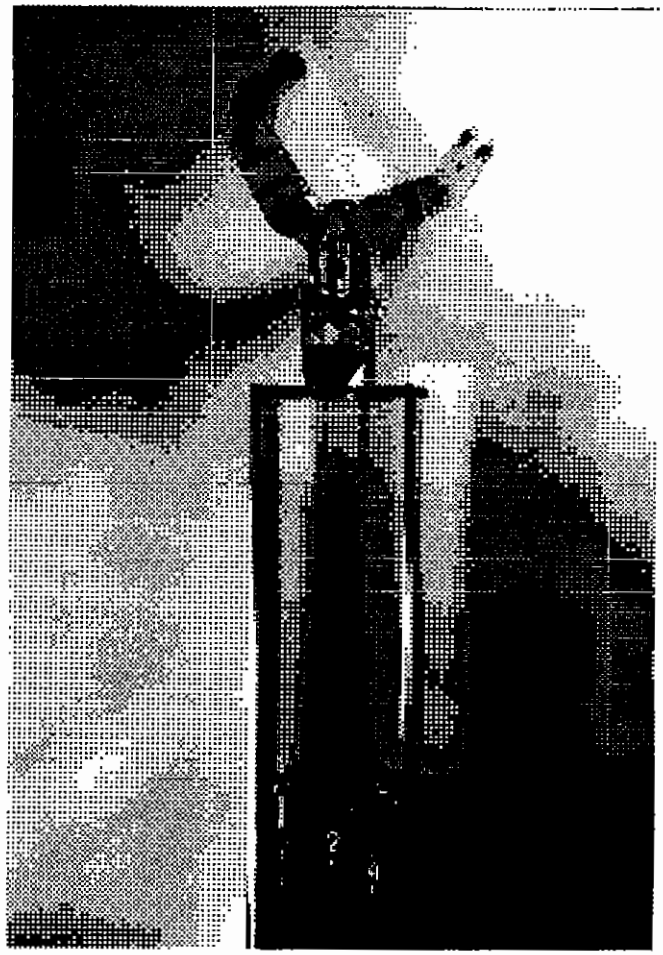

Figure 7.0.1. The Forearm Mockup with the Hand Prototype and the Actuator Package.

shaft. In fact, on more than one occasion, cables were found to have been riding shafts for several hours during testing of the hand. These cables showed signs of much surface abrasion, but when put back onto the pulleys, continued to work without any noticeable performance degradation or tendency to break. This suggests that the system is very resistant to abuse (and it has seen a lot in early testing). The pulley mounts will not be so indifferent to the cable's position, however, when they are being used as tendon tension sensors. Also, dropping cables will become much more of a nuisance when the actuator package is enclosed. In section 8.1 I present a suggestion for a pulley mount with a modified "cable keeper" to address this problem.

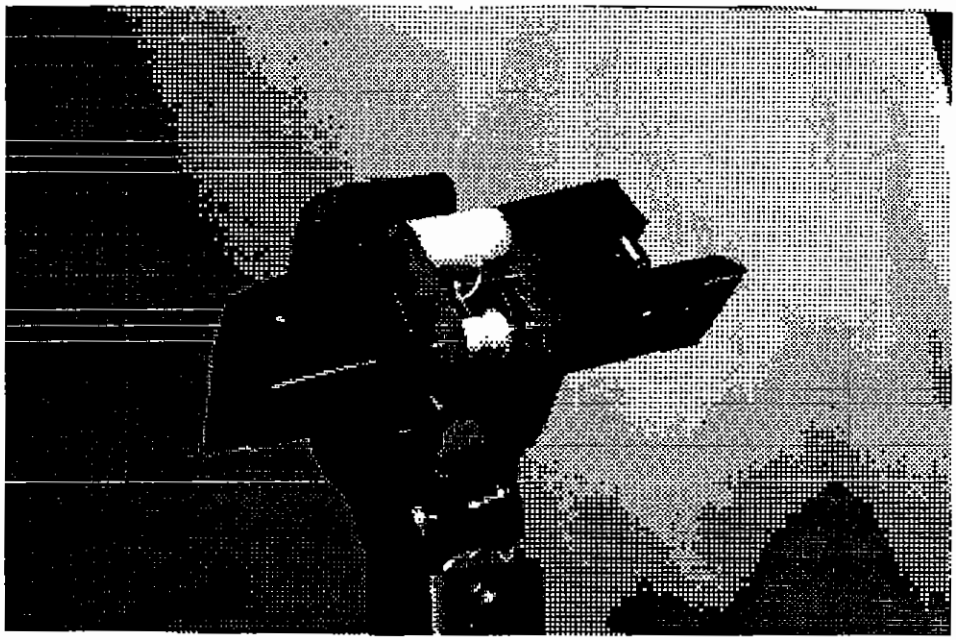

Figure 7.0.2. The Hand Grasping a Stapler

8.0 Future work.

The process of building and testing the prototype forearm has inspired some design revisions which may enhance the system. These design improvements are outlined here.

8.1 Pulley Keepers

While testing code, it became apparent that we need a way to ensure that the cables cannot come off the pulleys when they are allowed to go slack. One possible solution to this problem is to have a keeper surrounding the pulley so that when the cables go slack, they are confined to the space above the pulley groove. Upon retensioning, the cable will then reseat onto the pulley even if the cables have been moved while slack (see Figure 8.1.1). These will not, however, help to keep the cables seated properly on the wrist pulleys.

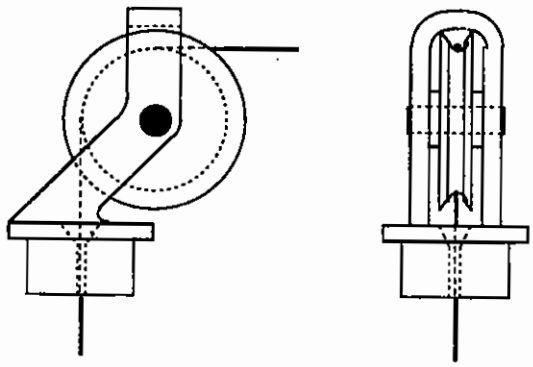

Figure 8.1.1. Pulley Mount with Keeper.

8.2 Slack Prevention Springs

The cable keepers would not be so important if the motor shafts could be biased with light springs which would take up the slack when the hand was powered down improperly. These "slack prevention" springs would also help keep the cables in place inside the wrist.

8.3 Cable passage in 3D

The cable routing was optimized in two dimensions without considering that cables could be crossed without interference if they were fed onto capstans at different levels from pulleys at different heights. The cable layout could be optimized in three dimensions, taking into account the positions of the cables as they exit the wrist.

8.4 Cable Experiments

Not enough data exists on small polymer braids for robot cables. Most of the fatigue life and self abrasion tests on these fibres have been run on large ropes meant for mooring boats. It is not clear that the data from these tests is applicable to small cables run inside robots, and more work needs to done in this area. Most notably, the compliance of the cables when being used as tendons is very important for force control, and should be studied more closely. Comparisons of fatigue, self abrasion, spring constants and different cable terminations need to be done before the potential of the new fibres can be fully realized.

8.5 Finishing the Wrist and Attaching it to the WAM

Once the hand has been finished and the final axis (roll) put on the wrist, the actuator package and the hand will be incorporated into a modular forearm which can be attached to the WAM (see Figure 8.3.1). This will add to the versatility of the WAM as a robot and provide a hardware platform for catching experiments and other control experimentation.

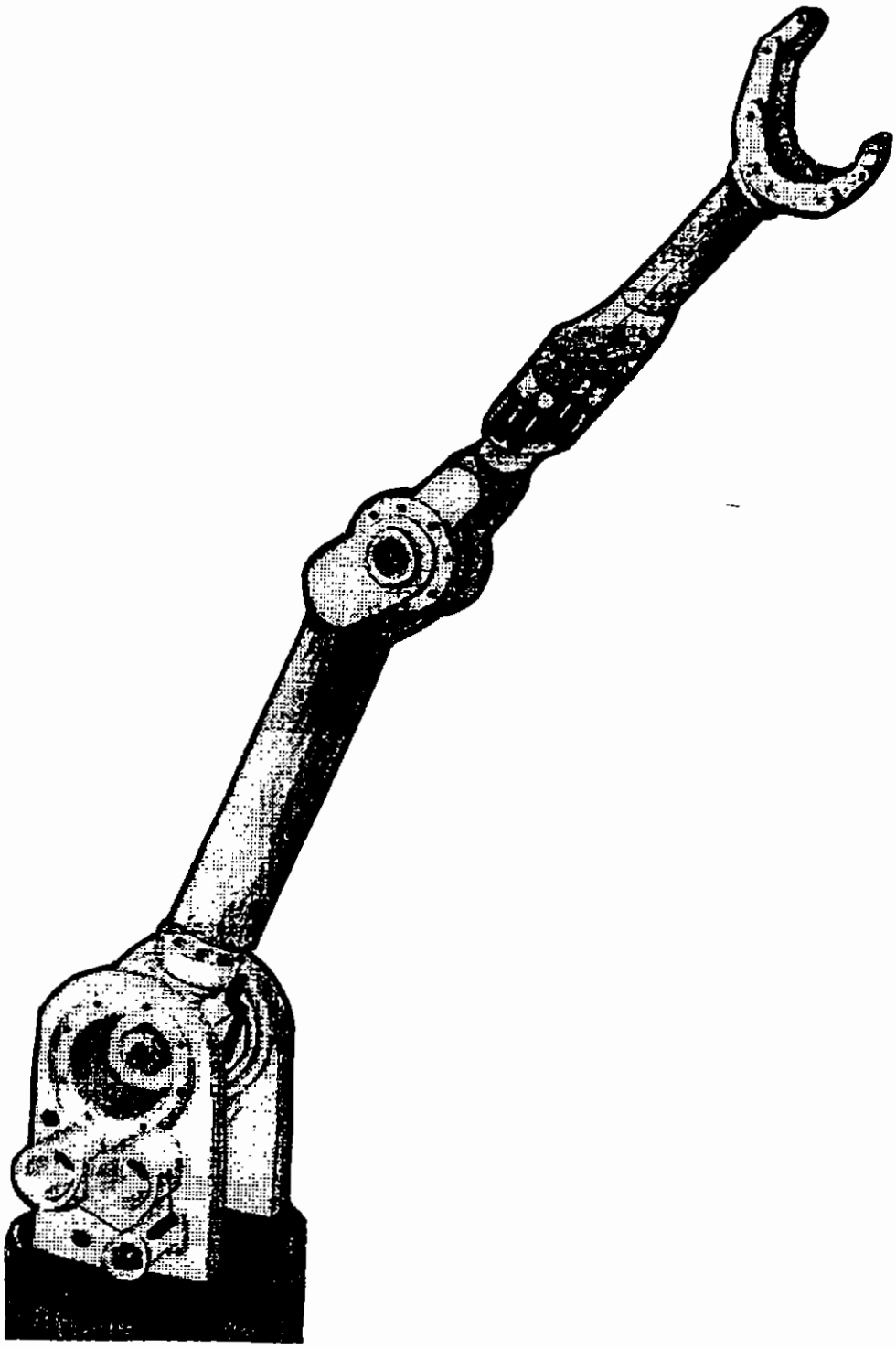

Figure 8.3.1. WAM with Proposed Forearm

Appendix A Motor data comparisons

		1	2	3	4
Motor Company Number		MT 1375-038	MT 1250-053	MT 1250-037	MT 1375-055
Max RPM		5691	5825	9549	4221
Max Torque T (oz-in)		11	11	6	22
T/W slope (calc)	T/RPM	1.93E-03	1.89E-03	6.28E-04	5.21E-03
Power Avail (Watts)		49	50	45	72
Max Temp (C)		155	155	155	155
TR/W (C/Watt)		7	7	9	6
Max cont. power (calc)	(Max temp - 25)/(TR/W)	19	19	14	22
Ripple Torque (%)		6	6	6	6
Rot inertia J (oz-in-sec^2)		3.60E-04	2.00E-04	1.00E-04	6.00E-04
Motor Friction		0.5	0.3	0.2	0.6
Operating Voltage (V)		39	37	31	41
Weight (oz)		1.40	2.10	1.20	2.20
OD (in)		1.375	1.250	1.250	1.375
Length (in)		0.380	0.540	0.380	0.550
Torque Sensitivity (ozin/amp)		8.86	8.15	4.14	12.50
hand effective mass M (slugs)		0.299	0.299	0.299	0.299
R Optimum (in)	(SQRT(J))/M	0.064	0.047	0.033	0.082
Amax	((T/SQRT(J))/(2*SQRT(M)))	530	712	549	822
Areq	2d/t^2	1067	1067	1067	1067
dmax		1.72	2.31	1.78	2.67
dreq	3"	3.00	3.00	3.00	3.00
Gear ratio rg (in)	max torque/640 oz	0.017	0.017	0.009	0.034
Result	if((amax>areq)and(rg>ropt))	FALSE	FALSE	FALSE	FALSE

Table A1. Motor Data Comparisons

5	6	7	8	9	10	11	12	13
MT 1500P-038	MT 1125D-037	MT 1500R-050	MT 1500P-051	MT 1500L-053	MT 1500L-069	MT 1937s-040	MT 1937s-053	MAX RE 10 37
6608	19580	4417	5193	4871	3982	5079	4465	4800
11	4	20	20	22	30	30	55	18
1.66E-03	2.04E-04	4.53E-03	3.85E-03	4.52E-03	7.53E-03	5.91E-03	1.23E-02	3.81E-03
56	57	69	82	91	95	120	120	10
155	155	155	155	155	155	155	155	100
7	11	6	6	6	6	6	6	19.40
19	12	22	22	22	24	22	22	4
7	7	5	7	6	6	6	6	NA
4.00E-04	5.00E-05	6.00E-04	5.00E-04	7.00E-04	1.10E-03	8.00E-04	1.30E-03	1.46E-04
0.6	0.25	0.7	0.7	0.8	1	1.8	2	0.1
33	36	45	39	35	34	37	41	18
1.40	1.40	2.30	2.20	2.00	2.80	3.00	4.40	4.59
1.500	1.125	1.500	1.500	1.500	1.500	1.935	1.935	0.984
0.388	0.375	0.510	0.515	0.530	0.690	0.400	0.530	2.146
6.42	2.54	12.90	9.56	9.32	11.10	9.30	11.50	2.31
0.299	0.299	0.299	0.299	0.299	0.299	0.299	0.299	0.299
0.067	0.024	0.082	0.075	0.089	0.111	0.095	0.121	0.040
503	518	747	818	761	828	970	1396	1384
1067	1067	1067	1067	1067	1067	1067	1067	1067
1.63	1.68	2.43	2.66	2.47	2.69	3.15	4.53	4.49
3.00	3.00	3.00	3.00	3.00	3.00	3.00	3.00	3.00
0.017	0.006	0.031	0.031	0.034	0.047	0.047	0.086	0.029
FALSE	FALSE	FALSE	FALSE	FALSE	FALSE	FALSE	FALSE	FALSE

14	15	16	17	18	19	20	21	22
MAX RE 20 38	INLAND QT-0717-E	INLAND QT-0707-A	INLAND QT-0706-B	INLAND QT-1106-A	INLAND QT-1204-B	-INLAND QT-1207-C	INLAND QT-1401-A	MicroMo 2842 36
10300	18350	8750	6858	6016	6924	5486	5269	5200
37	4	8	12	11	11	20	55	7
3.60E-03	2.09E-04	8.80E-04	1.79E-03	1.83E-03	1.59E-03	3.65E-03	1.04E-02	1.35E-03
20	53	50	63	49	57	82	217	7
125	155	155	155	155	155	155	155	125
19.40	45	33	25	19	25	19	15	18
5	3	4	5	7	5	7	9	6
NA	7	10	10	6	7	7	7	NA
1.30E-04	4.50E-05	1.10E-04	4.20E-04	3.20E-04	4.20E-04	6.00E-04	1.30E-03	2.22E-04
0.1	0.25	0.3	0.6	0.6	0.6	0.7	1.8	0.17
48	31	33	33	20	29	36	35	36
4.59	1.40	1.60	2.50	1.50	1.65	2.30	4.40	4.70
0.984	1.125	1.125	1.125	1.375	1.500	1.500	1.938	1.102
2.146	0.375	0.562	0.750	0.385	0.385	0.510	0.540	1.654
6.20	2.29	5.13	6.50	4.40	5.59	8.75	9.00	9.16
0.299	0.299	0.299	0.299	0.299	0.299	0.299	0.299	0.299
0.038	0.022	0.035	0.069	0.060	0.069	0.082	0.121	0.050
2976	524	672	549	563	491	747	1396	430
1067	1067	1067	1067	1067	1067	1067	1067	1067
9.66	1.70	2.18	1.78	1.83	1.59	2.43	4.53	1.40
3.00	3.00	3.00	3.00	3.00	3.00	3.00	3.00	3.00
0.058	0.006	0.012	0.019	0.017	0.017	0.031	0.086	0.011
TRUE	FALSE	FALSE	FALSE	FALSE	FALSE	FALSE	FALSE	FALSE

23	24	25	26	27	28	29	30	31
Clifton D-1375-A-1s	Clifton DPH-1650-A-1	Clifton D-1670-A-1	Clifton DBTH-2135-A-	Litton/Clifton AS-780D-17	Escap 28LT12-416E	Escap 28DT12-219E	Escap 28L28-416E	Hathway A-275 90
8513	3511	2956	8108	8922	7000	6650	5300	11
35	29	30	4	50	10	16	8	25
4.11E-03	8.26E-03	1.01E-02	5.18E-04	5.60E-03	1.40E-03	2.42E-03	1.47E-03	2.34E+00
223	113	80	17	168	13	20	8	79
150	*125*	*125*	*125*	155	155	155	155	180
11	*15*	*15*	*11*	10	17.00	11.50	17.00	*11*
11	7	7	9	13	8	11	8	14
7	10	na	na	7	na	na	na	NA
6.00E-04	9.00E-04	1.00E-03	1.00E-04	2.60E-04	2.52E-04	2.55E-04	2.48E-04	2.00E-04
1.5	1.5	*1.5*	*1.5*	1	*0.17*	*0.17*	*0.17*	1
38	36	20	54	24	32	28	24	36
2.50	5.30	3.00	4.00	6.80	4.76	7.05	4.41	5.50
1.375	1.650	1.670	1.562	1.312	1.102	1.102	1.102	1.550
0.550	1.638	0.567	1.062	1.902	1.622	2.465	1.575	2.400
6.00	13.00	9.00	8.90	3.64	6.10	5.52	6.09	11.70
0.299	0.299	0.299	0.299	0.299	0.299	0.299	0.299	0.299
0.082	0.100	0.106	0.033	0.054	0.053	0.053	0.053	0.047
1307	884	868	384	2837	565	922	453	1617
1067	1067	1067	1067	1067	1067	1067	1067	1067
4.24	2.87	2.82	1.25	9.21	1.83	3.00	1.47	4.96
3.00	3.00	3.00	3.00	3.00	3.00	3.00	3.00	3.00
0.055	0.045	0.047	0.007	0.078	0.015	0.025	0.012	0.039
FALSE	FALSE	FALSE	FALSE	TRUE	FALSE	FALSE	FALSE	FALSE

Appendix B More Mechanical Drawings.

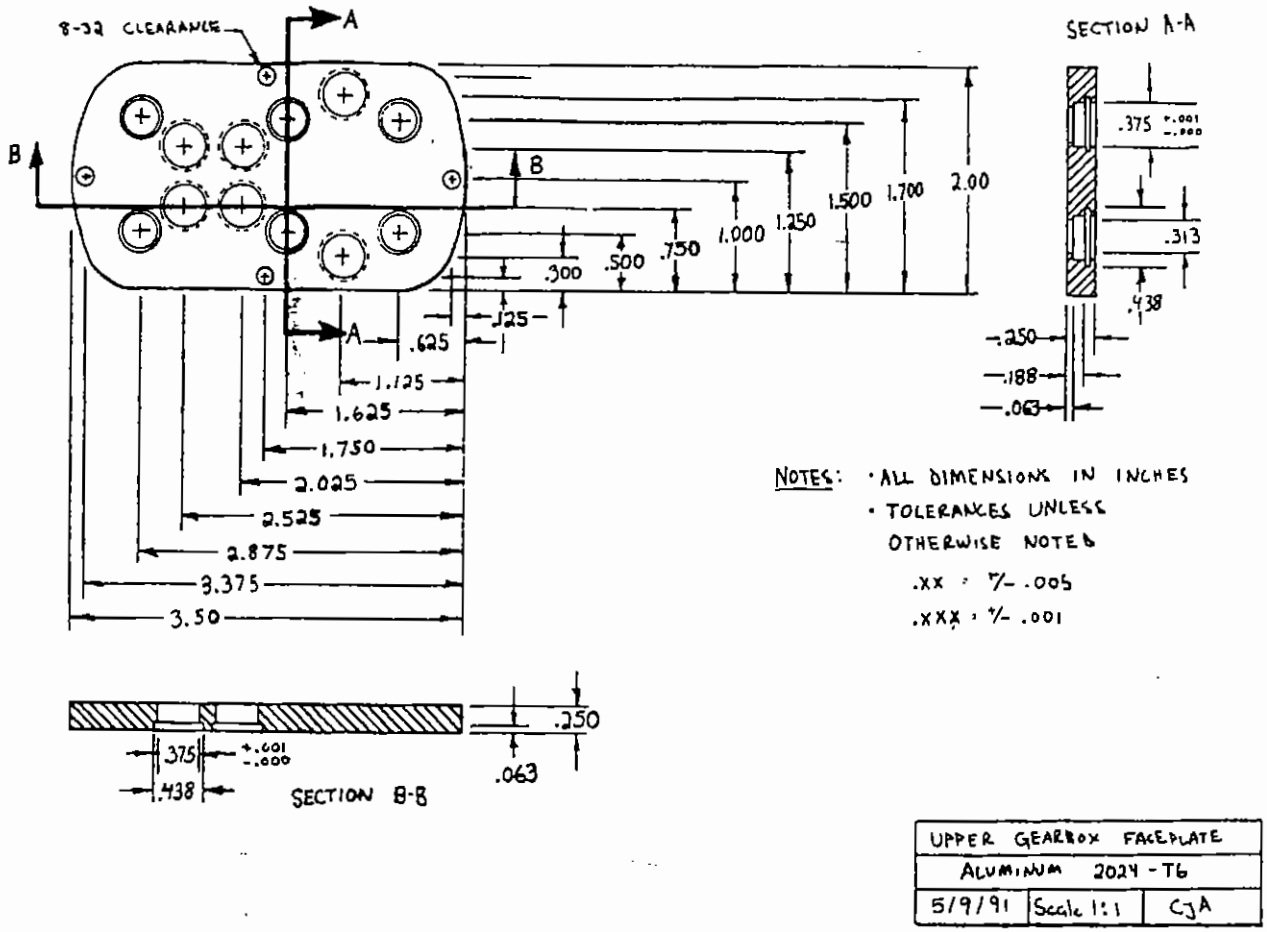

Figure A1. Upper Faceplate of the Actuator Package Gearbox

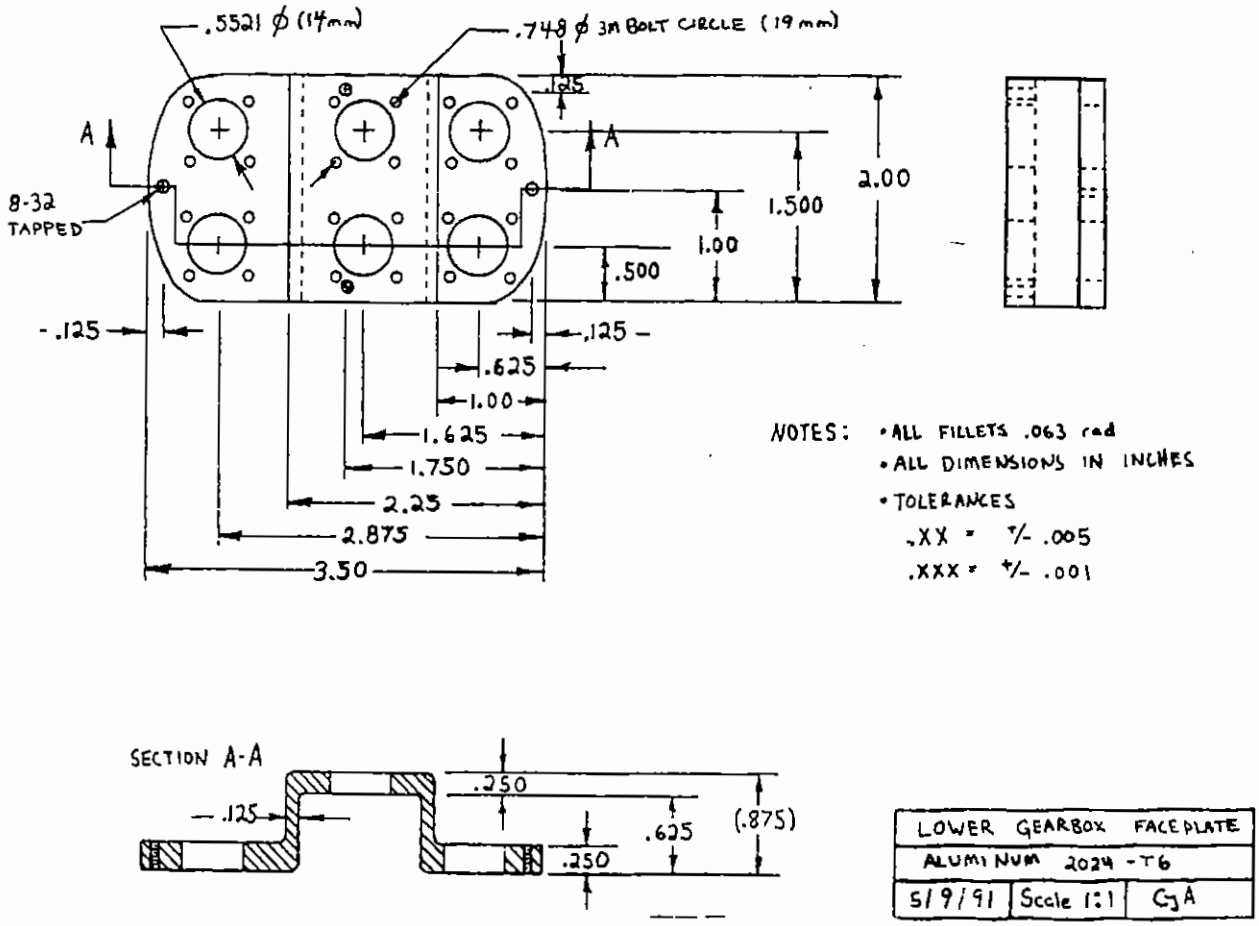

Figure A2. Lower Faceplate of the Actuator Package Gearbox

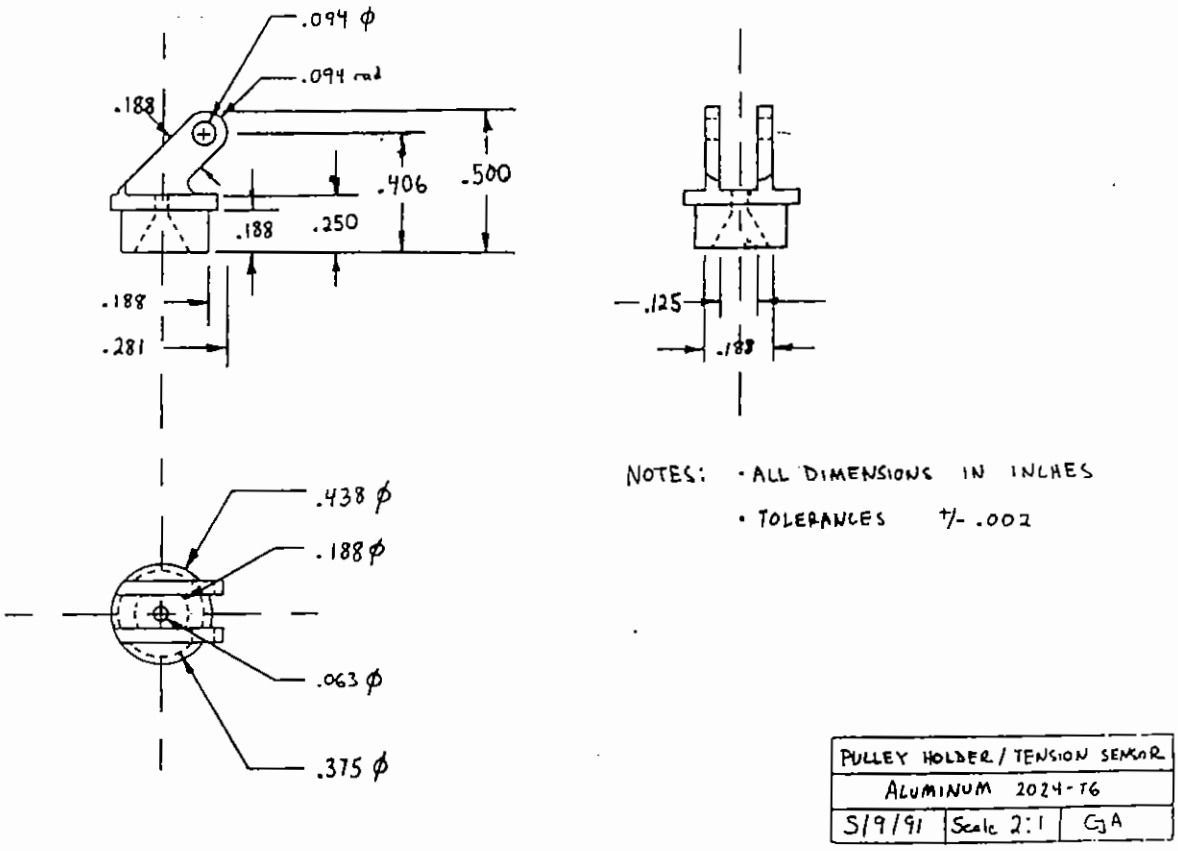

Figure A3. Pulley Mount

Bibliography

[Anderson, 90] Anderson, C. J. "The Design of a High-Torque/Low Speed Fractional Horsepower Generator/Motor Pair" B.S.M.E Thesis, Massachusetts Institute of Technology, January 1990.

[Arnold, 85] Arnold, Frank "Use Power Rate to Increase Machine Throughput and Reduce Power". *PCIM*, December 1985.

[Beers, 90] Beers, D.E. and Ramirez, J.E. "Vectran High-Performance Fiber". *Journal of the Textile Institute*.Vol. 81, No. 4, 1990.

[Bicchi, 90] Bicchi, A., Salisbury, J.K., and Brock, D.L. "Contact Sensing from Force Measurements" *A.I. Memo No. 1262*, October, 1990.

[Brock, 87] Brock, David L. "Enhancing the Dexterity of a Robot Hand Using Controlled Slip" M.S.M.E.Thesis, Massachusetts Institute of Technology, May 1987.

[Costello, 90]. Costello, George A. *Theory of Wire Rope*. Springer-Verlag, Inc: New York, 1990.

[Craig, 89] Craig, John J. *Introduction to Robotics Mechanics and Control 2nd Edition*. Addison Wesley Publishing Co.: Reading, MA 1989.

[DiPietro, 88] DiPietro, David M. "Development of an Actively Compliant Underwater Manipulator" SM Thesis, MIT/Woods Hole Joint Program Department of Oceanography and Oceanographic Engineering, May 1988.

[Eberman, 89] Eberman, Brian S. "Whole-Arm Manipulation: Kinematics and Control". M. S. Mechanical Engineering Thesis, Massachusetts Institute of Technology, 1989.

[Eppinger, 87] Eppinger, Steven D. Seering, Warren P. "Understanding Bandwidth Limitations in Robot Force Control" *IEEE International Conference on Robotics and Automation*. Raleigh, North Carolina., April 1987.

[Galasso, 89] Galasso, Francis S. *Advanced Fibres and Composites* . Gordon and Breach Science Publishers, N.Y. 1989.

[Greiner, 90] Greiner, Helen. "Passive and Active Grasping with a Prehensile Robot End-Effector". Masters Thesis, Massachusetts Institute of Technology May 1990.

[Hongu, 90] Hongu, Tatsuya and Philips, Glyn O. *New Fibres*. Ellis Horwood Limited: Chichester, England, 1990.

[Jacobsen, 86] Jacobsen, S.C., Iversen, E.K., Knutti, D.F. , Johnson, R.T., Biggers, K.B. "Design of the Utah/MIT Dexterous Hand" *Proc. IEEE International Conference on Robotics and Automation*, April 7-10, 1986.

[Jacobsen, 90] Jacobsen, S.C., Mladejovsky, M.G., Wood, J.E, and Wyatt, R.F. "Displacement Sensing by Direct Mechanical Modulation of Shaped Electro-Active Micro Structures" *IEEE Micro Electro Mechanical Systems*, 1990.

[Levin, 90] Levin, Michael D. "Design and Control of a Closed-Loop Brushless Torque Actuator." Masters thesis, Massachusetts Institute of Technology, May 1990.

[Mason and Salisbury, 85] Mason M.T., and Salisbury, J. K. *Robot Hands and the Mechanics of Manipulation.* MIT Press: Cambridge, MA, 1985.

[Moyer, 92] Moyer, Thomas H. "The Design of an Integrated Hand and Wrist Mechanism" Masters Thesis, Massachusetts Institute of Technology, Jan. 1992.

[Narasimhan, 87] Narasimhan, Sundar. "Dexterous Robotic Hands: Kinematics and Control". Masters Thesis, Massachusetts Institute of Technology, 1987

[Oberg, 85] Oberg, E., Jones, F. D., and Horton, H.L. *Machinery's Handbook 22nd Edition.* Henry Ryffel Ed. Industrial Press, Inc: New York, 1985.

[Pasch, 83] Pasch, Ken and Seering, W.P. "On the Drive Systems for High Performance Machines ".*Transactions of the ASME. Journal of Mechanisms, Transmissions and Automation in Design.*, Sept. 1983.

[Paul, 87] Paul, Benjamin J. "A Systems Approach to the Torque Control of a Permanent Magnet Brushless Motor" Masters Thesis, Massachusetts Institute of Technology. August, 1987.

[Sandvik] Sandvik, Inc. "Power Spring Designer's Guide". Sandvik Steel Company, Spring Products Division, Stranton, PA.

[Thompson, 90] Thompson, Bruce T. "The PHD: a Planar, Harmonic Drive Robot for Joint Torque Control". Masters Thesis, Massachusetts Institute of Technology, July, 1990.

[Townsend, 87] Townsend, W.T. and Salisbury, J.K. "The Effect of Coulomb Friction and Stiction on Force Control". *Proc. 1987 IEEE International Conference on Robotics and Automation,* Raleigh, NC. April 1987.

[Townsend, 88] Townsend, William T. "The Effect of Transmission Design on Force-Controlled Manipulator Performance". Ph. D Thesis, Massachusetts Institute of Technology, 1988.

[Townsend and Salisbury, 88] Townsend, W.T. and Salisbury J.K "The Efficiency Limit of Belt and Cable Drives". *Journal of Mechanisms, Transmissions, and Automation in Design*, Sept. 1988.

[Townsend, 89] Townsend, William T. and Salisbury, J. Kenneth. " *Mechanical Bandwidth as a Guideline to High-Performance Manipulator Design". Proceedings of IEEE international Conference on Robotics & Automation.* Phoenix, AZ, April 1989.

[Salisbury, 88] Kenneth Salisbury, William Townsend, Brian Eberman, and David DiPietro. "Preliminary Design of Whole-Arm Manipulation System (WAMS)". *Proceedings of the 1988 IEEE International Conference on Robotics and Automation.* Philadelphia, PA, April 24-29 1988.

[Ward, 89] Ward, Allen C. "A theory of Quantitative Inference Applied to a Mechanical Design Compiler". ScD Thesis, Massachusetts Institute of Technology, Jan 1989.

[Whitney, 87] Whitney, Daniel E. "Historical Perspective and State of the Art in Robot Force Control". *International Journal of Robotics Research.* Vol. 6. No. 1 Spring 1987.